Available online at www.sciencedirect.com

SCIENCE DIRECT®

Vision Research 44 (2004) 257–277

Vision Research

www.elsevier.com/locate/visres

Sensitivity to curvatures in orientation-based texture segmentation

Ohad Ben-Shahar *, Steven W. Zucker

Interdepartmental Neuroscience Program, Department of Computer Science, Yale University, New Haven, CT 06520, USA

Received 28 March 2003; received in revised form 12 August 2003

Abstract

Texture segregation has long been attributed to changes in the distribution of elementary features across the visual field [Nature 290 (12) (1981) 91; Biol. Cybernet. 54 (1986) 245]. The study of orientation, a conspicuous feature, has led to models of orientation-based texture segmentation (OBTS) that depend on the magnitude of one or two orientation gradients [Vis. Res. 31 (4) (1991) 679; Vis. Res. 31 (6) (1991) 1073] and influenced further by the relative configuration between the orientation textons and the global orientation edge [Percept. Psychophys. 52 (4) (1992) 255; Vis. Res. 35 (20) (1995) 2863]. Here we show that these models are at best partial and that the notion of orientation gradient has been incompletely used in the study of OBTS. To do so, we first study the behavior of orientation in orientation-defined texture patches. Geometrical analysis identifies two texture curvatures and reveals the incompleteness of previous stimuli. Psychophysical experimentation then demonstrates that segmentation is strongly affected by discontinuities in these curvatures. Importantly, we show that this sensitivity to curvature is independent of the orientation gradients and inconsistent with the simple configural considerations proposed in the past.

Keywords: Segmentation; Orientation; Curvature; Texture

1. Introduction

1.1. ODTs and OBTS

The visual perception of texture plays a fundamental role in many aspects of vision from figure-ground segregation to 3D shape and depth perception. The ability to effortlessly segregate texture stimuli into coherent parts has long been attributed to the changes in the spatial distribution of elementary features, sometimes called textons (Julesz, 1981, 1986). Of these features, one that has been studied extensively is orientation. While orientation-defined textures (ODTs) are frequent in natural and artificial visual stimuli (Fig. 1), textures are rarely characterized solely by orientation. Nevertheless, understanding the effect of orientation on texture segmentation is essential due to its neurophysiological basis (Hubel & Wiesel, 1977), its central role in perceptual organization (Kanizsa, 1979), and its close relationship to shape perception (Stevens, 1981; Todd & Reichel, 1990).

Orientation-defined textures in visual stimuli result from pattern formation processes that cover surfaces (and sometimes volumes) in the real world: fur might cover a bear; grass a field, or stripes a zebra. The visual appearance of these surfaces as ODTs is thus influenced by two basic factors: the behavior of the pattern formation processes and the interaction between surfaces during the imaging process. If follows that discontinuities in ODTs, and thus perceptual edges and OBTS in general, can arise in two fundamental ways.

The first cause of ODT discontinuities is occlusion of one (textured) object by another; each textured surface projects to an ODT region that meets the other along the occlusion boundary. This rather common scenario raises the question of how the ODT varies in the neighborhood of the occlusion boundary. Computational studies show that there are two possible generic events, and that they can be classified as folds and cuts (Huggins & Zucker, 2001), as is illustrated in Fig. 2.

The pattern formation processes that cover surfaces in the real world often enjoy smoothness properties. However, they need not be smooth everywhere. This observation leads us to the second cause of discontinuities—those that result from singularities in the pattern formation processes themselves. This issue is studied

* Corresponding author.
E-mail address: ben-shahar@cs.yale.edu (O. Ben-Shahar).

0042-6989/$ - see front matter © 2003 Elsevier Ltd. All rights reserved.
doi:10.1016/j.visres.2003.08.018

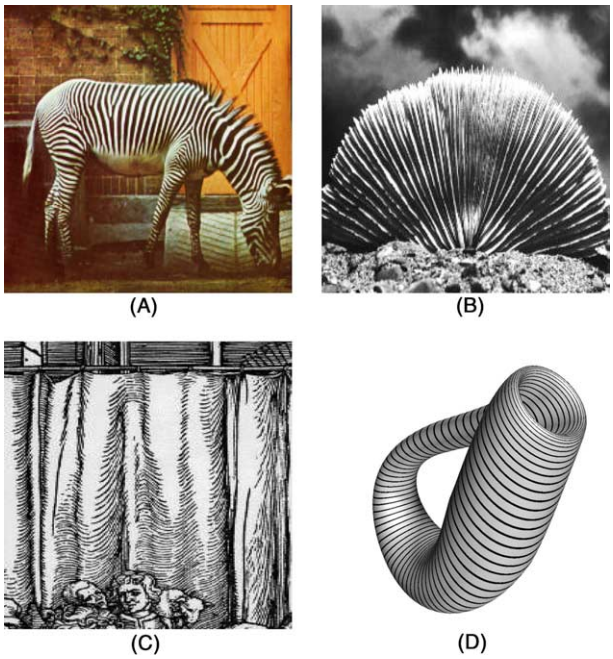

Fig. 1. ODTs are frequent in natural stimuli, the visual arts, technical drawings, and other visual artifacts. In all cases, ODTs are rarely constant since this requires an accidental match between the surface geometry, the texture formation process, and the observer's view-point. (A) Zebra's stripes. (B) Sea shell. (C) Woodcut by Dürer (cropped from Kruth, 1963, panel 175). (D) A technical drawing of a Klein bottle (courtesy of Paul Bourke, Swinburne University of Technology, Australia).

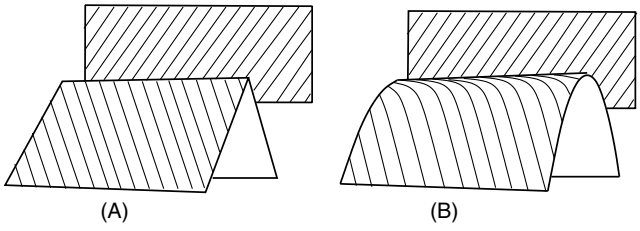

Fig. 2. Cuts and folds as generic events near occlusion boundary (reproduced from Huggins & Zucker, 2001). (A) A generic cut event implies that the ODT intersects the occlusion boundary transversely. (B) A generic fold event implies that the ODT approaches a tangent configuration with the occlusion boundary. Note that this happens whether or not the texture on the surface has constant orientation.

extensively in the formation of biological patterns and morphogenesis (Corbit & Garbary, 1995; Murray, 1989; Turing, 1952) and is well exemplified by the singularities in the striped patterns that cover, for example, both zebras and many sea shells (Fig. 1). Importantly, it suggests that interesting (singularity) events can occur in ODTs that lead to a variety of configurations, none of which can be classified as occlusion boundaries.

Regardless of the process that creates ODT discontinuities, one universal property holds for all—natural ODTs are seldom constant in the neighborhood of discontinuities. In fact, every-day ODT stimuli are not likely to have constant orientation even *within* coherent regions; this requires an accidental match between the surface geometry, the texture formation process, and the observer's view-point (Fig. 1). Furthermore, perspective projection dictates that even completely parallel lines in the world are likely to give rise to a non-constant retinal ODT. Since ODTs are generically not constant, either within coherent regions or in the neighborhood of orientation edges, it is noteworthy that much of their psychophysical investigation in the last two decades has focused on stimuli of piecewise constant orientation (Caputo, 1997; Caputo & Casco, 1999; Kwan & Regan, 1998; Landy & Bergen, 1991; Li, 1998; Motoyoshi & Nishida, 2001; Nothdurft, 1985a; Regan, Hajdur, & Hong, 1996; Wolfson & Landy, 1995, 1998). Part of our goal in this paper is to bring this larger context to the fore, both computationally and psychophysically.

1.2. OBTS and orientation gradients

Although orientation and ODTs are geometrical objects, the study of OBTS has exploited very little of their intrinsic geometry. Filter-based approaches (e.g., Landy & Bergen, 1991; Malik & Perona, 1990) consider the geometrical content only as a basis for computing scalar energies from which segmentation is derived through nonlinear transformation (typically, rectification) and detection of areas of high gradient. Feature-based models (Mussap & Levi, 1999; Nothdurft, 1991, 1993) suggest more generally that OBTS depends on the relationship between two orientation gradients (Fig. 3), namely—the change in orientation *between* coherent regions ($\Delta\theta_{\text{between}}$) and the change in orientation *within* regions ($\Delta\theta_{\text{within}}$). As expected, the former must be significantly larger than the latter for segmentation to occur.

Although the notion of orientation gradient (sometimes called orientation contrast) is invoked by most models for OBTS, the fact that gradients are *vector* quantities is typically overlooked. In particular, although orientation gradients, like any other gradient, have both magnitude and direction, their directional property is generally ignored. This may be justifiable in the case of $\Delta\theta_{\text{between}}$ since it describes the change of orientation across 1D perceptual edges. The same cannot be said about $\Delta\theta_{\text{within}}$, though, since it is supposed to characterize the behavior of orientation in 2D regions. Thus, whenever the vectorial nature of $\Delta\theta_{\text{within}}$ becomes important, we use the mathematical gradient symbol $\nabla\theta$ instead. [1] In other cases we use the symbol $\Delta\theta_{\text{within}}$ but

[1] This and all other symbols used in this paper are summarized in Appendix A.

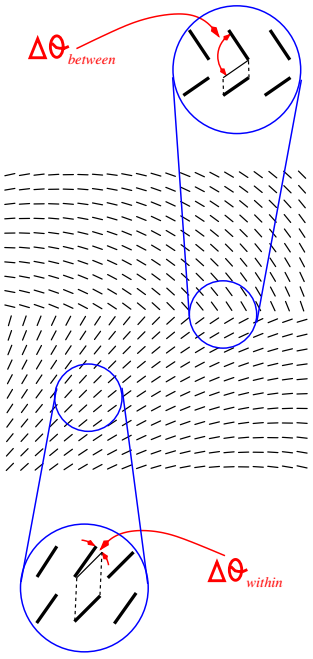

Fig. 3. Existing models (Landy & Bergen, 1991; Mussap & Levi, 1999; Nothdurft, 1991) predict that OBTS depends on the relationship between two orientation gradients, one within and the other between perceptually coherent regions. These models predict that segmentation occurs reliably if and only if the ratio $\frac{\Delta\theta_{\text{between}}}{\Delta\theta_{\text{within}}}$ is significantly larger than 1.

we also keep in mind that it is defined as the magnitude of $\nabla\theta$, i.e., $\Delta\theta_{\text{within}} \triangleq \|\nabla\theta\|$.

This sharper semantics calls for investigating the relationship between $\nabla\theta$ (as a vector) and performance in OBTS. Indeed, contrary to predictions from existing models, changing only the *direction* of $\nabla\theta$ (without changing its magnitude, $\Delta\theta_{\text{within}}$), carries significant perceptual consequences (Fig. 4). In fact, we found that perceptual differences exist even for a fixed combination of $\nabla\theta$ and $\Delta\theta_{\text{between}}$ (Fig. 5). One must conclude that other factors also play a role in OBTS.

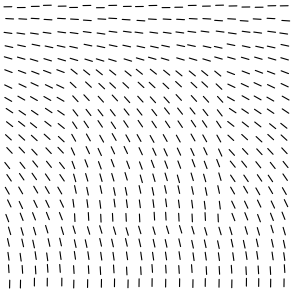

Fig. 5. Another demonstration that not only $\Delta\theta_{\text{between}}$ and $\Delta\theta_{\text{within}}$ determine the perceptual outcome of OBTS. In this stimulus $\nabla\theta$ (and thus, $\Delta\theta_{\text{within}}$) is constant within the figure and within the ground, and $\Delta\theta_{\text{between}} = 18°$ is constant across the figure's edges (a square). Nevertheless, the saliency of the top edge is significantly higher than that of the bottom edge, which is hardly detectable without scrutiny. Note that since the orientation texels along one side of the bottom edge are exactly perpendicular to it, the fact that it is less salient relative to the top edge justifies a closer reexamination of previous predictions (Wolfson & Landy, 1995). In particular, it raises the possibility that configural effects are themselves modulated by ODT variations.

1.3. Overview

The goal of this paper is to present a computational and psychophysical study of OBTS in the larger (and more realistic) context of spatially varying ODTs. To do so, and to adequately capture the variability of ODTs, we first formally analyze ODTs from a geometrical point of view. We identify two curvature measures that suggest new intrinsic factors in OBTS and lead to

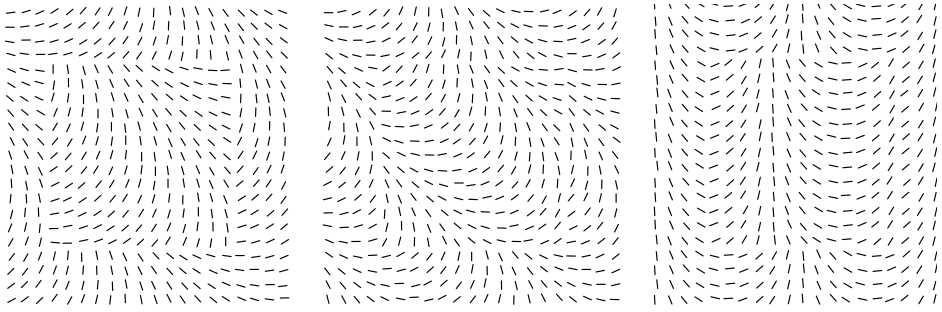

Fig. 4. Orientation gradients are not enough to predict OBTS. (A) Inspired by Nothdurft (1991), this stimulus has a clear orientation-defined figure segmented away from its ground, both of which have the same orientation gradient $\nabla\theta$ within their interior. Here $\nabla\theta = \frac{(45°,45°)}{\sqrt{32}}$ and its magnitude is $\Delta\theta_{\text{within}} = 11.25°$. Consistent with existing models, the large orientation discontinuity of $\Delta\theta_{\text{between}} = 90°$ across the figure's boundary induces easy segmentation. (B) Still consistent with current models, the segmentation of the same figure becomes more difficult as the ratio $\frac{\Delta\theta_{\text{between}}}{\Delta\theta_{\text{within}}}$ decreases. Here $\nabla\theta = \frac{(18°,18°)}{\sqrt{2}}$, $\Delta\theta_{\text{within}} = 18°$, and $\Delta\theta_{\text{between}} = 36°$. However, this case also reveals that the saliency of the square's boundary is not uniform (compare its lower left corner to the upper right one) and suggests that segmentation may be influenced by more than the scalar values of $\Delta\theta_{\text{within}}$ and $\Delta\theta_{\text{between}}$. (C) The last hypothesis is further emphasized by rotating the direction of $\nabla\theta$. Now, the orientation gradient vector points horizontally, $\nabla\theta = (18°, 0°)$ but its magnitude is still $\Delta\theta_{\text{within}} = 18°$ and $\Delta\theta_{\text{between}}$ is still 36°. Nevertheless, the overall perceptual effect is very different. In particular, note how the saliency of the left and right boundaries has diminished almost completely despite the fact that the orientation discontinuity across them is identical to that across the top and bottom boundaries.

rigorous psychophysical investigation of their effect. The results of our experiment demonstrate how segmentation can be strongly affected by discontinuities in these curvatures independently of the two orientation gradients $\Delta\theta_{\text{within}}$ and $\Delta\theta_{\text{between}}$.

The introduction of ODT curvatures greatly extends the possibilities for modeling OBTS, by including sensitivity to curvature discontinuities and its interaction with other known factors. At the same time, it allows keeping such models within the realm of *intrinsic* data that can be measured locally. Indeed, the model that emerges from our experiment predicts previously observed configural effects (Nothdurft, 1992; Olson & Attneave, 1970; Wolfson & Landy, 1995) which, due to their extrinsic nature, cannot be developed into computationally predictive models. At the same time, our results also suggest subtle inconsistencies with these configural effects. In the second part of this paper we analyze all these considerations in detail, both theoretically and experimentally. We conclude that OBTS cannot be explained based on orientation gradients and configural effects only, but rather that both orientation, curvatures, and "mixing" properties must be considered.

2. The intrinsic geometry of ODTs

Observe first that the internal representation of ODTs in the visual system, and thus their abstract representation, is likely to be dense, or continuous, as opposed to discrete (Fig. 6A). Formally, a 2D orientation function $\theta(x,y)$, which described the ODT orientation at each point, may be sufficient (Fig. 6B). However, this representation does not provide enough insight into the intrinsic geometry. As Marr has strongly advocated (Marr, 1982), different representations make explicit different properties and types of information. Indeed, an abstraction that emphasizes the intrinsic geometry and also provides an object-centered view is the *frame-field representation* (O'Neill, 1966).

Applying this framework from differential geometry, we place a suitable coordinate frame $\{\widehat{\mathbf{E}}_{\mathrm{T}}, \widehat{\mathbf{E}}_{\mathrm{N}}\}$ at each point $\vec{\mathbf{q}} = (x,y)$ of the texture and examine how this frame changes as a small translation $\vec{\mathbf{V}}$ is made from the point $\vec{\mathbf{q}}$. A suitable frame in the case of ODTs is one whose vectors are tangent ($\widehat{\mathbf{E}}_{\mathrm{T}}$) and normal ($\widehat{\mathbf{E}}_{\mathrm{N}}$) to the texture's orientation (Fig. 6C). Note that $\widehat{\mathbf{E}}_{\mathrm{T}}(\vec{\mathbf{q}})$ is drawn at the angle $\theta(\vec{\mathbf{q}})$—the local orientation at point $\vec{\mathbf{q}}$ relative to a fixed horizontal axis. The initial change (i.e., rotation) in the frame as it is translated from $\vec{\mathbf{q}}$ along direction $\vec{\mathbf{V}}$ is expressed via the *covariant derivatives* (do Carmo, 1976; Koenderink, 1990; O'Neill, 1966) of the underlying pattern. These covariant derivatives, $\nabla_{\vec{\mathbf{V}}}\widehat{\mathbf{E}}_{\mathrm{T}}$ and $\nabla_{\vec{\mathbf{V}}}\widehat{\mathbf{E}}_{\mathrm{N}}$, are naturally represented as vectors in the basis $\{\widehat{\mathbf{E}}_{\mathrm{T}}, \widehat{\mathbf{E}}_{\mathrm{N}}\}$:

$$\begin{pmatrix} \nabla_{\vec{\mathbf{V}}}\widehat{\mathbf{E}}_{\mathrm{T}} \\ \nabla_{\vec{\mathbf{V}}}\widehat{\mathbf{E}}_{\mathrm{N}} \end{pmatrix} = \begin{bmatrix} 0 & w_{12}(\vec{\mathbf{V}}) \\ -w_{12}(\vec{\mathbf{V}}) & 0 \end{bmatrix} \begin{pmatrix} \widehat{\mathbf{E}}_{\mathrm{T}} \\ \widehat{\mathbf{E}}_{\mathrm{N}} \end{pmatrix}. \tag{1}$$

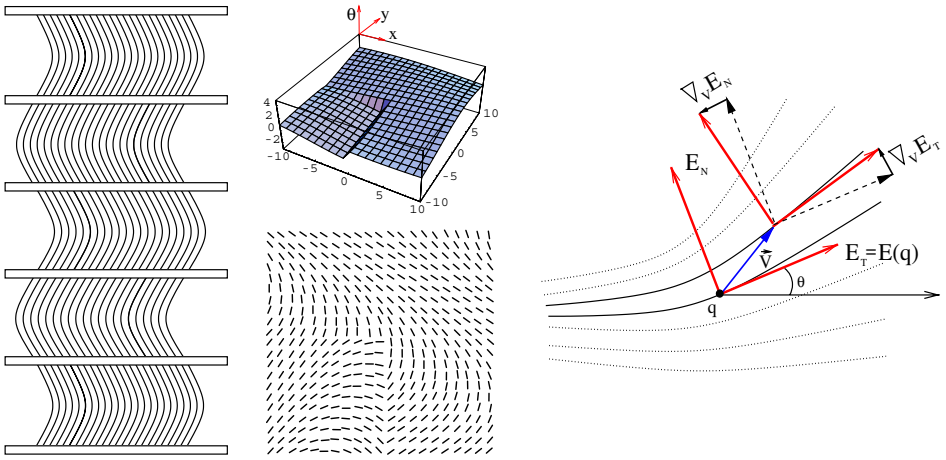

Fig. 6. Abstract representations of orientation-defined textures. (A) This ODT is amodally completed behind the occluders and is perceived as a single coherent texture. This occurs even though the different segments of the texture contain different numbers of texture lines. Thus, the completion cannot be that of individual curves, which suggests that internally, our visual system maintains a representation for orientation that is *dense*. (B) Abstractly, a dense representation for orientation implies a 2D orientation function which associates an orientation to each point $\vec{\mathbf{q}} = (x,y)$ in the image (retinal) plane. Such functions can be visualized as surfaces whose height represents orientation. In such a representation, perceptual orientation edges are depicted as abrupt height change (compare height function at the top to its corresponding texture on the bottom). (C) A frame field representation of orientation-defined texture and its covariant derivatives. At each point $\vec{\mathbf{q}}$ a suitable frame $\{\widehat{\mathbf{E}}_{\mathrm{T}}, \widehat{\mathbf{E}}_{\mathrm{N}}\}$ is placed on the texture. As we shift from the point $\vec{\mathbf{q}}$ along direction $\vec{\mathbf{V}}$, the frame rotates. This change is captured by the covariant derivative of the pattern which can be expressed in terms of the frame via the connection equation. Such a representation reveals two curvatures which characterize the local behavior of the texture's orientation from an object-centered point of view.

This system—Cartan's *connection equation* (Koenderink, 1990; O'Neill, 1966)—involves the linear *connection form* $w_{12}(\vec{\mathbf{V}})$ which can be represented in terms of $\{\widehat{\mathbf{E}}_T, \widehat{\mathbf{E}}_N\}$:

$$w_{12}(\vec{\mathbf{V}}) = w_{12}(a\widehat{\mathbf{E}}_T + b\widehat{\mathbf{E}}_N) = aw_{12}(\widehat{\mathbf{E}}_T) + bw_{12}(\widehat{\mathbf{E}}_N).$$

The local behavior of ODTs is thus governed by two scalars at each point. We define them as follows:

$$\begin{aligned} \kappa_T &\triangleq w_{12}(\widehat{\mathbf{E}}_T), \\ \kappa_N &\triangleq w_{12}(\widehat{\mathbf{E}}_N) \end{aligned} \tag{2}$$

and interpret them as *tangential* and *normal* curvatures, respectively, since they represent the initial rate of change of orientation in the tangential and normal directions, respectively. These curvatures are not only intrinsic (i.e., independent of particular parametrization and invariant under Euclidean transformations in the retinal plane) to the ODT, they also make explicit the spatially varying nature of ODTs and emphasize the restricted nature of classical (constant) ODT stimuli.

The two curvatures κ_T and κ_N can be expressed directly in terms of the orientation function $\theta(x,y)$ and its gradient $\nabla\theta$

$$\begin{aligned} \kappa_T &= \nabla\theta \cdot (\cos\theta, \sin\theta), \\ \kappa_N &= \nabla\theta \cdot (-\sin\theta, \cos\theta), \end{aligned} \tag{3}$$

which in turn shows that the previously used $\Delta\theta_{\text{within}}$ can be expressed directly in terms of curvatures:

$$\Delta\theta_{\text{within}} = \|\nabla\theta\| = \sqrt{\kappa_T^2 + \kappa_N^2}. \tag{4}$$

Since the frame field point of view results in two curvatures at each point of the ODT, across the structure we obtain two scalar fields, i.e., two curvature *functions*. Not unlike the Gaussian and mean curvatures of surfaces, these two curvature functions are not completely independent. In particular, curvatures of valid ODTs with orientation function $\theta(x,y)$ must satisfy the following covariation constraint:

$$\nabla\kappa_T \cdot \widehat{\mathbf{E}}_N - \nabla\kappa_N \cdot \widehat{\mathbf{E}}_T = \kappa_T^2 + \kappa_N^2. \tag{5}$$

This integrability constraint suggests that unlike curvature (κ) and torsion (τ) for curves, not every combination of ODT curvatures will integrate into a valid ODT. One particular important consequence of this observation is that unless both these curvatures are identically zero (as in a constant ODT), neither they, nor the ODT orientation, can be simultaneously constant in *any* ODT patch, however small (Ben-Shahar & Zucker, 2003). Thus, in general, at least one of the ODT curvatures must vary, or the two curvatures need to covary, in any neighborhood of the ODT.

Eq. (3) is extremely important in the context of OBTS because it implies that the *same* orientation gradient $\nabla\theta$ can give rise to *different* combinations of curvatures (e.g., by changing θ without changing $\nabla\theta$), and thus can give rise to different combinations of curvature discontinuities along perceptual orientation edges. The analogy to the perceptual evidence (Figs. 4 and 5) therefore raises the possibility that OBTS may relate to texture curvatures and their discontinuities, subject to the constraint in Eq. (5). Our main goal in this paper is to explore this possibility from a psychophysical point of view.

3. Experiment 1—Sensitivity to curvature in OBTS

To explore the role of curvature discontinuities in OBTS we conducted a two-alternative forced choice texture segmentation experiment with stimuli designed specifically to test segmentation performance as a function of $\nabla\theta$, $\Delta\theta_{\text{between}}$, and the discontinuities (or contrast) in the texture curvatures, $\Delta\kappa_T$ and $\Delta\kappa_N$. This section describes this experiment and its results.

3.1. Stimuli overview

All stimuli consisted of ODTs which were portrayed as arrays of 21×21 bright oriented segments on black background. [2] Viewed by subjects from an approximate distance of 1 m, all stimuli spanned 10° of visual angle. Each ODT contained two lines of orientation discontinuity—one diagonal and one horizontal—which together defined a perceptual "figure"; either a left-pointing or a right-pointing triangle (Fig. 7). The oriented segments were initially positioned along a regular grid of 10×10 degrees and then randomly jittered up to 5′ in each direction to avoid grid artifacts.

Similar to previous experiments (Landy & Bergen, 1991; Mussap & Levi, 1999; Nothdurft, 1985a, 1985b; Nothdurft, 1991; Wolfson & Landy, 1995), we designed the figure and ground to have a fixed orientation contrast (i.e., $\Delta\theta_{\text{between}}$ is constant along the figure's boundaries in any given trial). Following past studies with textures of *varying* orientations (Mussap & Levi, 1999; Nothdurft, 1991, 1992), we also set the orientation gradient *within* the figure and the ground to be constant (i.e., $\nabla\theta_{\text{figure}} = \nabla\theta_{\text{ground}} = \nabla\theta =$ constant in any given trial).

Unlike previous experiments, however, we also designed our stimuli to have constant *curvature* discontinuities. In other words, both $\Delta\kappa_T$ and $\Delta\kappa_N$—the jump in

[2] Although other methods to depict ODTs have also been used in the past (Landy & Bergen, 1991), the use of discrete oriented texels predominates the OBTS literature (Mussap & Levi, 1999; Nothdurft, 1991, 1992, 1993; Wolfson & Landy, 1995) and it allowed us a better comparison to previous studies with everywhere changing ODTs (Mussap & Levi, 1999; Nothdurft, 1992, 1993).

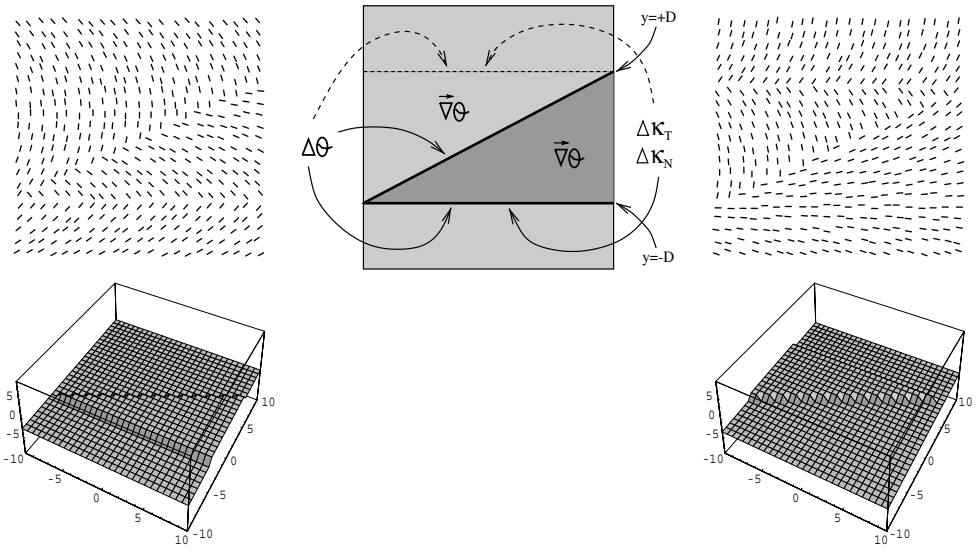

Fig. 7. Basic stimulus design. The subject's task was to identify one of two possible orientation-defined figures, either a left-pointing (left) or a right-pointing (right) triangle. The *same* diagonal discontinuity appeared in all stimuli and thus played no role in the subject's decision. Along the other edge (either at top or bottom), all of $\Delta\theta_{\text{between}}$, $\Delta\kappa_T$, and $\Delta\kappa_N$ were constant (within a trial). $\nabla\theta$, the orientation gradient, was also constant (within each trial) and identical for both the figure and the ground. Two examples are shown, both as ODTs and 3D surfaces (*a la* Fig. 6B). Both stimuli have $\nabla\theta = (0°, 5°)$ and $\Delta\theta_{\text{between}} = 75°$. To optimize printing, stimuli are shown in reversed contrast. Those used in the experiment had bright segments on dark background.

tangential and normal curvatures, respectively—were constant (within a trial) between the figure and the ground along their defining horizontal edge (Fig. 7). Fortunately, the iso-curvature curves of ODTs with constant $\nabla\theta$ are straight lines, thus designing stimuli with constant curvature discontinuities is computationally feasible (see Section 3.2). To avoid compromising the explored psychophysical measures, and to allow for meaningful conclusions on configural effects (see Sections 4 and 5), all stimuli were designed to have an orientation gradient $\nabla\theta$ of a carefully selected (vertical) direction, which resulted in a one-to-one mapping between $\nabla\theta$ and the previously used $\Delta\theta_{\text{within}}$. Therefore, in the following we use them interchangeably.

For each combination of $\nabla\theta$ and $\Delta\theta_{\text{between}}$, three different combinations of $\Delta\kappa_T$ and $\Delta\kappa_N$ were tested. Note that once $\nabla\theta$, $\Delta\theta_{\text{between}}$, and *one* $\Delta\kappa$ is set, the other $\Delta\kappa$ is fully determined from Eq. (3), as is dictated by Eq. (5) (see Section 3.2). The chosen combinations of $\Delta\kappa_T$ and $\Delta\kappa_N$ covered three fundamental behaviors for the curvatures. One was defined by $\Delta\kappa_T = 0$, the second by $\Delta\kappa_N = 0$, and the third by $\Delta\kappa_T = \Delta\kappa_N$. In other words, the first class of orientation discontinuities had no discontinuity in tangential curvature, the second lacked discontinuities in normal curvatures, and the last was characterized by (the same) discontinuity in both curvatures (Fig. 8). Note again that such triples of stimuli were created for *each* combination of $\nabla\theta$ and $\Delta\theta_{\text{between}}$, thus allowing us to investigate the effect of curvature discontinuities *independently* of the orientation gradients.

3.2. Stimuli details

Once the jittered position of the texels was set, their orientation was calculated from the underlying orientation function of the region they belonged to

$$\begin{aligned}\theta_{\text{ground}}(x,y) &= \theta_0 + \Delta\theta_{\text{within}} \cdot y,\\ \theta_{\text{figure}}(x,y) &= \theta_0 + \Delta\theta_{\text{within}} \cdot y + \Delta\theta_{\text{between}}.\end{aligned} \tag{6}$$

Each stimulus had a fixed combination of $\Delta\theta_{\text{within}}$ and $\Delta\theta_{\text{between}}$ chosen from the following sets:

$$\Delta\theta_{\text{within}} \in \{5°, 10°, 15°, 20°, 25°, 30°\},$$
$$\Delta\theta_{\text{between}} \in \{5°, 10°, 15°, \ldots, 85°, 90°\}.$$

The free parameter θ_0 was set such that the corresponding curvature functions κ_T and κ_N achieved predefined discontinuities along a given horizontal line positioned at $y = \pm D$, where D corresponds to 2.5° (Fig. 7). Since the two curvatures are coupled through Eqs. (3) and (5), only one discontinuity is needed (say $\Delta\kappa_T$) to fully determine the other and thus fully determine θ_0. With the center of the stimulus as the origin, the solution to θ_0 takes the following form:

$$\theta_0 = -\frac{1}{2}\left[\Delta\theta_{\text{between}} + 2\sec^{-1}\left(\frac{2\Delta\theta_{\text{within}}\sin\frac{\Delta\theta_{\text{between}}}{2}}{\Delta\kappa_T}\right) + 2D\Delta\theta_{\text{within}}\right]. \tag{7}$$

Since we seek only real solutions, the trigonometric component of the last expression defines limits on the possible curvature discontinuities:

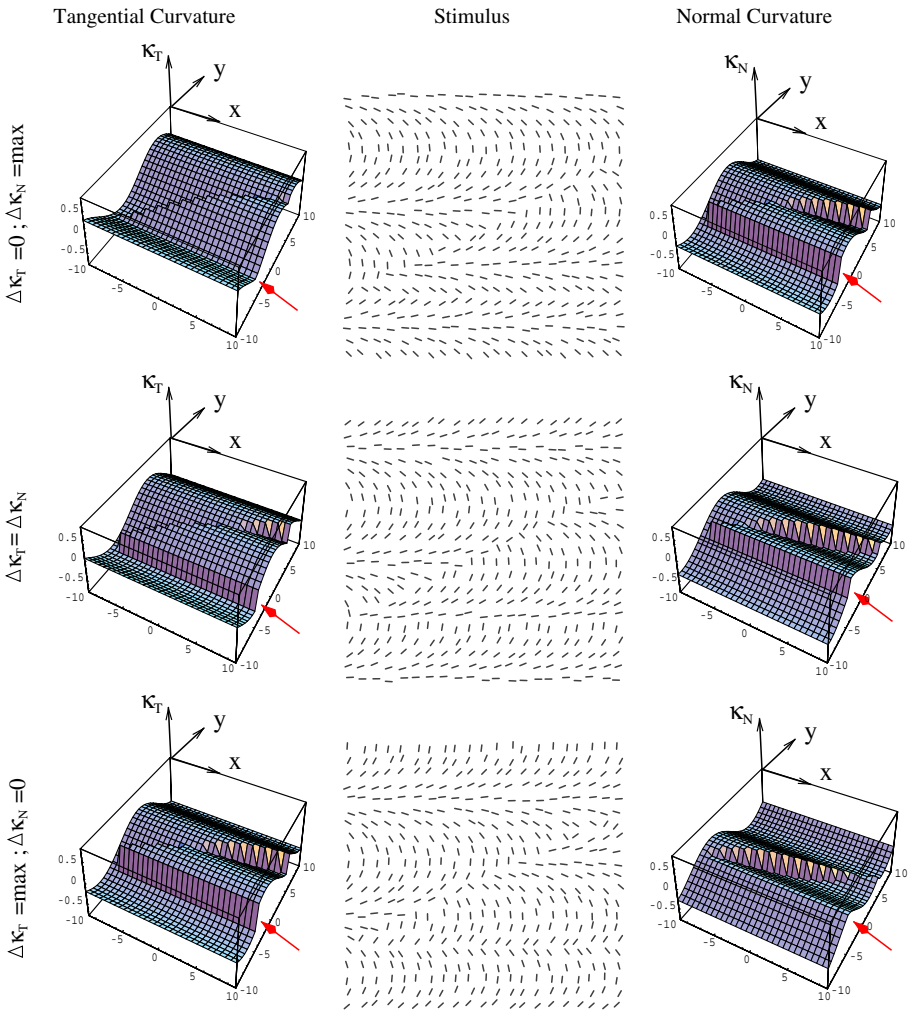

Fig. 8. Illustration of the three cases of curvature discontinuities examined in our experiment. For each combination of $\nabla\theta$ and $\Delta\theta_{\text{between}}$, three cases of curvature discontinuities were formed. Here we show the three cases for a left pointing triangle with $\Delta\theta_{\text{within}} = 20°$ and $\Delta\theta_{\text{between}} = 90°$. The 3D graphs show κ_{T} and κ_{N} as height functions over the image domain. The red arrows mark the discontinuities in curvatures, which are depicted, when present, as an abrupt change in height. Note how no discontinuity in one curvature (e.g., $\Delta\kappa_{\text{T}} = 0$) implies a large (in fact, the largest possible) discontinuity in the other curvature. Since the diagonal discontinuity remains fixed across the different triangles, the variation in $\Delta\kappa_{\text{T}}$ and $\Delta\kappa_{\text{N}}$ along it is irrelevant to the subject's decision.

$$|\Delta\kappa| \leqslant \Delta\kappa_{\max} \triangleq 2\Delta\theta_{\text{within}} \sin\left(\frac{\Delta\theta_{\text{between}}}{2}\right). \tag{8}$$

This limit thus defines the three possible combinations for the curvature discontinuities which we used in the experiment

$$\begin{aligned} &\Delta\kappa_{\text{T}} = 0 \Rightarrow \Delta\kappa_{\text{N}} = \Delta\kappa_{\max}, \\ &\Delta\kappa_{\text{T}} = \Delta\kappa_{\text{N}} \Rightarrow \Delta\kappa_{\text{T}} = \Delta\kappa_{\text{N}} = \frac{\Delta\kappa_{\max}}{\sqrt{2}}, \\ &\Delta\kappa_{\text{N}} = 0 \Rightarrow \Delta\kappa_{\text{T}} = \Delta\kappa_{\max}. \end{aligned} \tag{9}$$

With θ_0 set and plugged into Eq. (6), segments were plotted as antialiased lines centered at their jittered positions and having length of 25′. All stimuli were precomputed and stored before the beginning of the experiment and later displayed on a high-resolution flat color monitor (Dell UltraScan P991) using a 1 GHz Pentium-III PC.

3.3. Subjects and procedure

Six subjects (five naive, one author) participated in this experiment. All subjects had normal or corrected-to-normal vision and each ran six sessions of 1080 trials (total of 6480 trials). Sessions were run on successive days and each consisted of 10 blocks of 108 trials (separated by short breaks). Each session lasted for an hour and included one or two practice blocks of 72 trials.

Each trial started with a 600 ms presentation of a mask (ODT of randomly oriented segments), followed by 200 ms of brief stimulus presentation and another 500 ms of post-stimulus mask. (Stimulus presentation

was set to 200 ms to approximately average presentation time from previous related studies; 160 ms in Nothdurft (1992) and 250 ms in Wolfson and Landy (1995).) A post-marker prompted the subject to choose either a left- or right-pointing triangle. Each stimulus (i.e., a particular combination of $\Delta\theta_{\text{within}}$, $\Delta\theta_{\text{between}}$, and $\Delta\kappa_{\text{T}}$ and $\Delta\kappa_{\text{N}}$) was presented 20 times, 10 for each of the two possible figures, and their order was randomized and set before the experiment. To prevent observer strategies involving scrutinizing parts of the display, stimuli were randomly jittered up to $\pm 1.5°$ in each direction. During debriefing, all subjects reported using no special strategy other than global judgment in making their decisions.

3.4. Results

If current models of OBTS of non-constant ODTs were valid (Mussap & Levi, 1999; Nothdurft, 1991), varying the behavior of curvature across the figure/ground boundary while holding $\nabla\theta$ and $\Delta\theta_{\text{between}}$ fixed should lead to no differences in segmentation performance. While Nothdurft (1992) demonstrated configural variations that affect segmentation performance in the presence of fixed $\Delta\theta_{\text{within}}$ and $\Delta\theta_{\text{between}}$, (see below) here we show that similar conclusions can be drawn based on curvature discontinuities (i.e., based on intrinsic parameters only).

We first analyzed our data while pooling over the curvature dimension to control for, and replicate, existing findings. The results (Fig. 9) agree qualitatively with previously reported performance (Mussap & Levi, 1999; Nothdurft, 1991) and indicate that on average, segmentation accuracy decreases with larger $\Delta\theta_{\text{within}}$ and smaller $\Delta\theta_{\text{between}}$. Reliable segmentation occurs only when the ratio $\frac{\Delta\theta_{\text{between}}}{\Delta\theta_{\text{within}}}$ is sufficiently larger than 1. The detection thresholds (75% detection accuracy) that we obtained $\left(\frac{\Delta\theta_{\text{between}}}{\Delta\theta_{\text{within}}} \approx 7\right)$ were higher than those reported in the past due to the different stimuli, procedure, and other experimental parameters that we used.

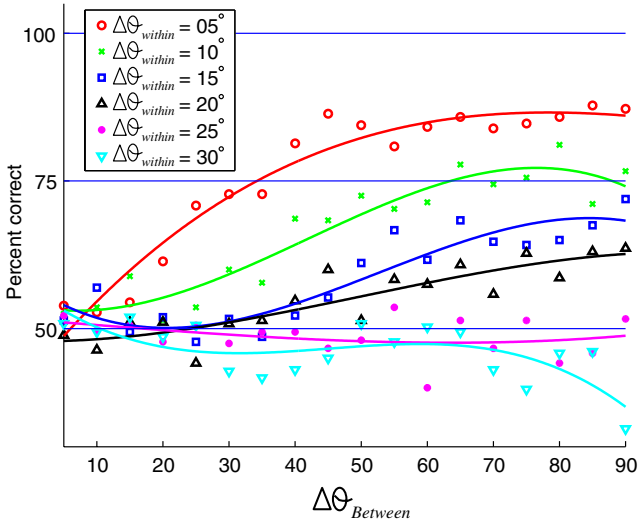

Fig. 9. Average accuracy of OBTS plotted against figure/ground orientation contrast ($\Delta\theta_{\text{between}}$). Different colors represent the accuracy for different values of $\Delta\theta_{\text{within}}$. Note how performance decreases with larger $\Delta\theta_{\text{within}}$ and smaller $\Delta\theta_{\text{between}}$. Here, as well as in subsequent figures, graphs are third order polynomials fitted to the data.

Taking curvature into account, however, reveals a different and intriguing pattern because the different curvature-based classes of orientation discontinuities produce *significant and consistent differences* in segmentation performance (Fig. 10). Three qualitative observations follow from such a curvature-based analysis. First, for small $\nabla\theta$ ($\Delta\theta_{\text{within}} \leqslant 10°$), segmentation of discontinuities with $\Delta\kappa_{\text{T}} = 0$ (red graphs) was substantially inferior. In fact, subjects were able to reliably detect this class of discontinuities only for $\Delta\theta_{\text{within}} \leqslant 5°$ and $\Delta\theta_{\text{between}} \geqslant 75°$. $\Delta\theta_{\text{within}}$ greater than 5° prevented any segmentation of this class of discontinuities, regardless of $\Delta\theta_{\text{between}}$. Secondly, for intermediate $\nabla\theta$ values ($15° \leqslant \Delta\theta_{\text{within}} \leqslant 20°$), the only detectable class of orientation discontinuities was the one which was discontinuous in *both* curvatures (green graphs). This superior performance was found to be statistically significant both on average (Fig. 11) and individually for each $\Delta\theta_{\text{between}}$ beyond the detection threshold (not shown for space considerations). Finally, the largest $\nabla\theta$ values ($\Delta\theta_{\text{within}} \geqslant 25°$) collapse all cases to chance level, indicating that OBTS is uniformly impossible for this class of patterns.

It is particularly instructive to examine the differences in segmentation performance between discontinuity classes in light of the average performance for each $\Delta\theta_{\text{within}}$ (Fig. 9). For example, the blue graph in Fig. 9 that corresponds to average performance with $\Delta\theta_{\text{within}} = 15°$ shows no crossing of the 75% detection threshold. However, splitting this average into its components (Fig. 10, left panel on second row) reveals that this low average is dominated by the two discontinuity classes of $\Delta\kappa_{\text{T}} = 0$ and $\Delta\kappa_{\text{N}} = 0$, both of which are hardly raised above chance level. But to conclude that no reliable segmentation is possible at $\Delta\theta_{\text{within}} = 15°$ is clearly incorrect as the $\Delta\kappa_{\text{T}} = \Delta\kappa_{\text{N}}$ graph in this category shows excellent segmentation performance for $\Delta\theta_{\text{between}} \geqslant 50°$. Since the $\Delta\kappa_{\text{T}} = \Delta\kappa_{\text{N}}$ class of discontinuities was typically the most salient for the smaller values of $\nabla\theta$ too, we conclude that, in general, orientation discontinuities of equal orientation contrast are *not* all perceptually equivalent and that those with $\Delta\kappa_{\text{T}} = \Delta\kappa_{\text{N}}$, where the discontinuities in κ_{T} and κ_{N} are maximized simultaneously, are the most salient ones.

Finally, it was observed that our displays occasionally incorporated certain horizontal configurations

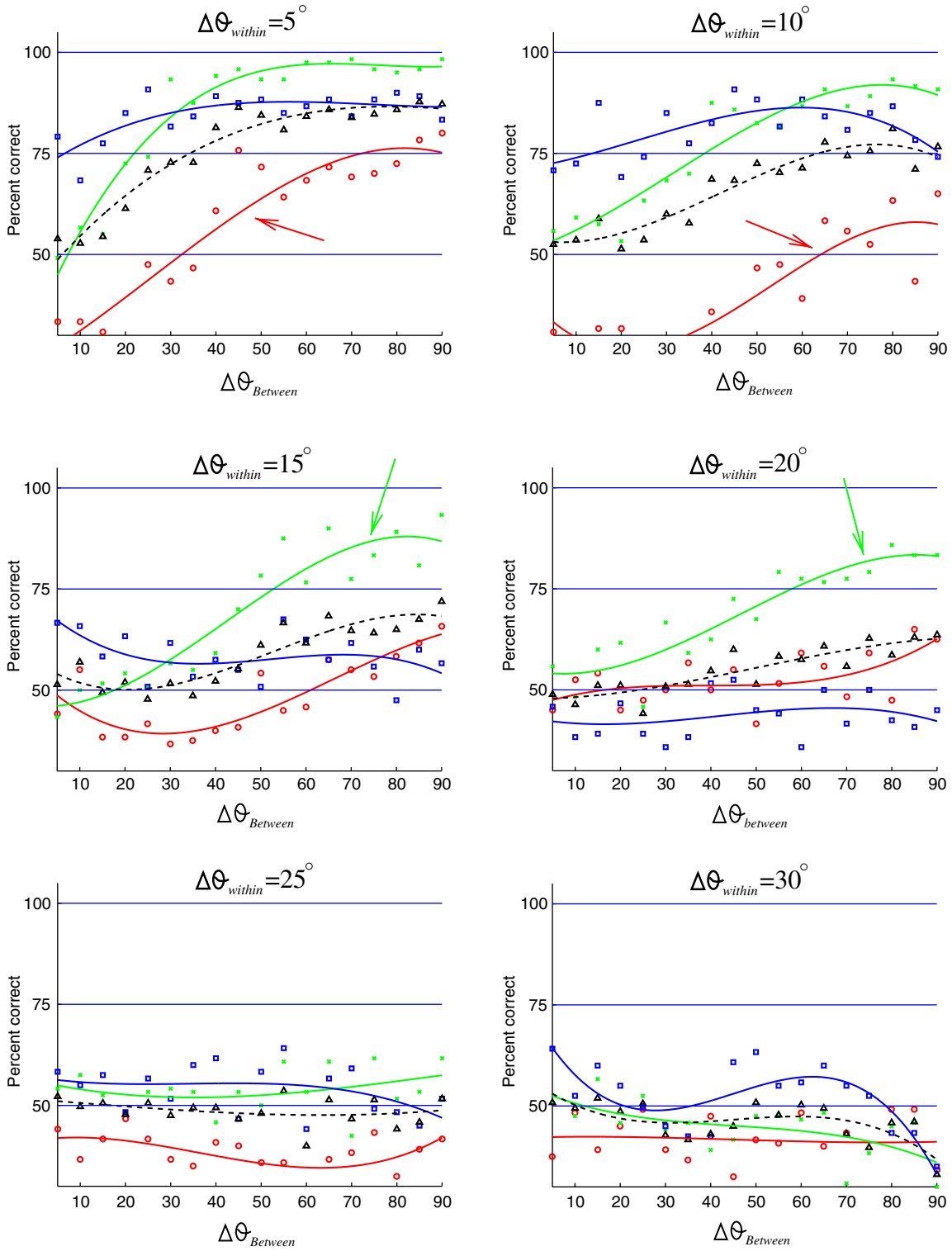

Fig. 10. Orientation-based segmentation accuracy plotted against figure/ground orientation contrast ($\Delta\theta_{\text{between}}$). Segmentation performance as a function of both $\Delta\theta_{\text{between}}$ and curvature discontinuities. Each panel corresponds to a different value of $\Delta\theta_{\text{within}}$. Red graphs correspond to $\Delta\kappa_{\text{T}} = 0$ discontinuities. Blue graphs correspond to $\Delta\kappa_{\text{N}} = 0$ discontinuities. Green graphs correspond to discontinuities with $\Delta\kappa_{\text{T}} = \Delta\kappa_{\text{N}}$. Dashed black graphs are the average for each case (replicated from Fig. 9). Note how the different curvature classes produce markedly different graphs. In particular, for small gradients ($\Delta\theta_{\text{within}} \leqslant 10°$), $\Delta\kappa_{\text{T}} = 0$ discontinuities (graphs marked with red arrows) are much less salient while for intermediate gradients ($15° \leqslant \Delta\theta_{\text{within}} \leqslant 20°$) only discontinuities of $\Delta\kappa_{\text{T}} = \Delta\kappa_{\text{N}}$ cross the detection threshold (graphs marked with green arrows). At higher gradients, all classes collapse to chance level.

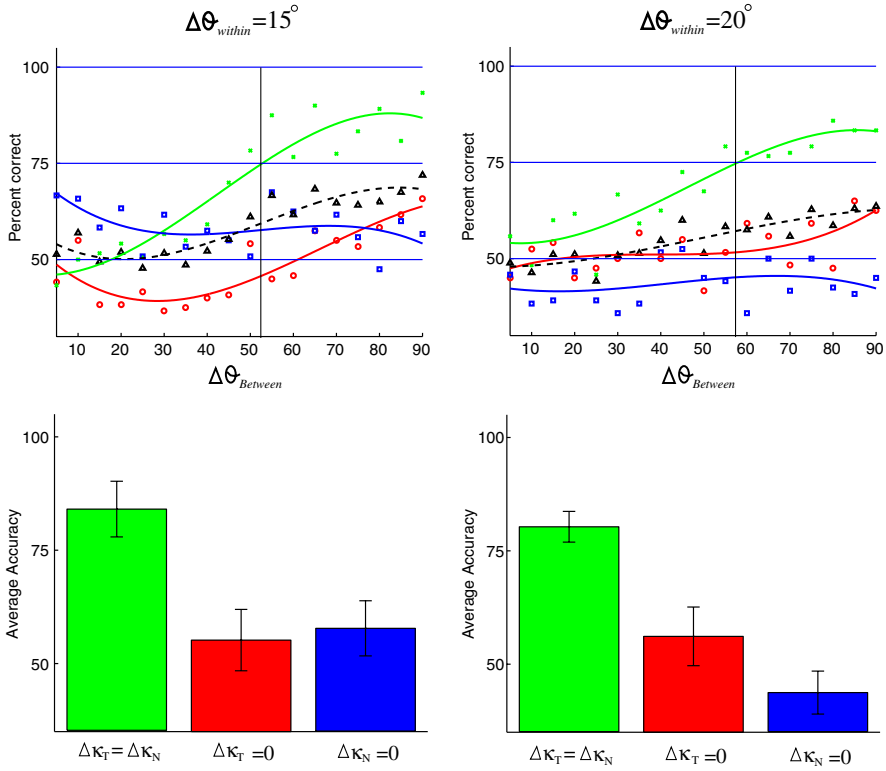

Fig. 11. When the $\Delta\kappa_T = \Delta\kappa_N$ class of discontinuities is superior to the others ($15° \leqslant \Delta\theta_{within} \leqslant 20°$), the differences in detection accuracies are statistically significant. Since an unbiased indicator for superiority in performance is signaled by the 75% accuracy threshold, we checked the statistical differences between the cases by identifying this threshold for the graphs that crossed them (marked by the black vertical lines) and collecting all data points beyond it. The two bar plots show the averages of these data sets for both $\Delta\theta_{within} = 15°$ and 20°. Error bars represent ± 1 standard error. In both cases, the difference between the $\Delta\kappa_T = \Delta\kappa_N$ mean (green) and the other two is highly significant ($p < 0.001$).

("kinks") in their smooth parts, that could have served as a segmentation cue and possibly bias observers' response. We thus exhaustively examined our set of (648) different stimuli to evaluate the extent, and possible effect, of these structures on overall subject's performance. We have found that in general subjects' response was independent (i.e., both "correlated" and "anti-correlated") of the existence of these structures; that significant differences in segmentation performance between the three curvature-based cases were evident even when *no* "kink" features were present in the stimuli; and that significant differences in segmentation performance were evident even when "kink" features were equally frequent in all of the cases. Only when $\Delta\theta_{within}$ was 10° and $\Delta\theta_{between}$ smaller than 50°, could such "kinks" in the $\Delta\kappa_T = 0$ stimuli possibly have biased subjects response consistently to less-than-chance level performance (see top right panel of Fig. 10). Although the exact nature of this particular phenomenon is still unclear, it is possibly related to the "edge hallucination" phenomenon reported by Nothdurft (1992).

3.5. Discussion—ODT curvatures and configural effects

The results of Experiment 1 show that OBTS clearly is affected by more than just the orientation gradients $\Delta\theta_{within}$ and $\Delta\theta_{between}$, and suggest that curvature discontinuities can play a major role in segmentation performance. Factors other than $\Delta\theta_{within}$ and $\Delta\theta_{between}$ that affect OBTS were previously observed psychologically (Olson & Attneave, 1970), but have been barely explored systematically. The main related observation was made by Wolfson and Landy who found that OBTS is improved if the "orientation of texels [is] parallel, and to some extent perpendicular, to the [orientation defined] texture edge" (Wolfson & Landy, 1998, p. 2876).

This observation is significant because the configural factor it refers to relates directly to the generic cut and fold organizations we described earlier (Section 1.1; Fig. 2). Equally important is what is missing from this observation, namely, $\nabla\theta$ and $\Delta\theta_{between}$. In other words, it suggests that the configuration around the orientation edge affects its saliency, but that this effect is independent of the orientation gradients.

While the lack of dependency on orientation gradients may be a direct outcome of the constrained piecewise-constant ODTs that Wolfson and Landy (1995) experimented with, their observation that "OBTS is improved if the orientation of texels [is] parallel, and to some extent perpendicular, to the texture edge" already makes predictions about intermediate configurations rather difficult. In Fig. 5, for example, the top (salient)

edge of the square is defined by an orientation jump from 27° to 45°, while the bottom (hardly seen) edge is defined by an orientation jump from 90° to 108°. Thus, the top edge is much further from a "parallel configuration" than the bottom one is from a "perpendicular configuration". Why, then, is the top edge significantly more salient than the bottom one? Could the spatially varying nature of this ODT contribute to the perceptual outcome?

To the best of our knowledge, the only systematic study of configural effects in spatially varying ODTs was carried out by Nothdurft (1992). Employing methods from his earlier studies (Nothdurft, 1985a, 1991), Nothdurft systematically examined OBTS performance as a function of the *average* configuration of the figure's texels relative to the figure/ground boundary. Predating Wolfson and Landy (1995), he too observed a "systematic dependence of correct bar detection on the alignment of border and element orientations", albeit with no contribution from perpendicular configurations. Unfortunately, Nothdurft (1992) examined only ODTs of one particular $\Delta\theta_{\text{within}}$, leaving open the question about the interaction of this parameter with configural effects in OBTS. Furthermore, his choice of the direction of $\nabla\theta$ relative to the orientation edges in the stimuli introduced deviations of up to 30° from the desired configuration (texels either parallel or perpendicular to the edge), thus incorporating a significant amount of uncertainty into the results. (Deviations up to 13.3° from the studied configuration were also present in Wolfson and Landy (1995).)

Another important aspect of the similar observations made by Nothdurft (1992) and Wolfson and Landy (1995) is that both are based on, and phrased in terms of, the orientation edge itself. Wolfson and Landy (1995) go a step further by proposing a computational "energy model that can account (for the detection of the edge and its saliency) by giving extra weight to the oriented channel which is oriented similarly to the edge". Unfortunately, such an explanation introduces a chicken-and-egg problem; the outcome (i.e., the orientation edge) must be given as an input to the computational process from which it is supposed to emerge (and after all, the goal of OBTS is to find these edges). Wolfson and Landy recognized this as well, and commented that a model that takes into account the orientation of the texture edge (or any other aspect of it) is "not particularly compelling" (Wolfson & Landy, 1995, p. 2872). Indeed, an appropriate model should rely on intrinsic data only and should predict configural modulations as a side effect.

The above discussion raises a question about our stimuli: have all of the interacting factors in defining our ODTs—the positions, orientations, and curvatures—somehow conspired to work together in an unanticipated way, for example by producing edge configurations for which configural effects were already observed. Two principle outcomes are possible. First, we might find that our curvature-based findings are indeed simply a rephrasing of the previously observed configural effects. Such an outcome is not undesired; it will imply that all existing findings can be explained based on intrinsic measurements only, thus avoiding the chicken-and-egg problem.

Alternatively, we might find that our curvature-based findings are incompatible with the previously reported configural effects. Such an outcome will have significant consequences of a different flavor: it will suggest that previously observed configural effects are not universally true and that they interact with orientation gradients and ODT curvatures.

While Fig. 5 implies that configural factors *may* be modulated by ODT variations, Fig. 8 suggests that at least in some cases, the salient $\Delta\kappa_{\text{T}} = \Delta\kappa_{\text{N}}$ condition produces a parallel/perpendicular configuration at the orientation edge. Fig. 12 further implies that this correspondence is independent of $\Delta\theta_{\text{within}}$ and thus not accidental, at least when $\Delta\theta_{\text{between}} = 90°$. All this conflicting evidence suggests that a thorough examination of the relationship between configural effects and our curvature-based findings is required. The rest of this paper is devoted to this issue, which we address both computationally and psychophysically. The conclusion that emerges is that previously observed configural effects are, in fact, incompatible with the results based on curvature, and that they are modulated by ODT variations in the proximity of orientation edges.

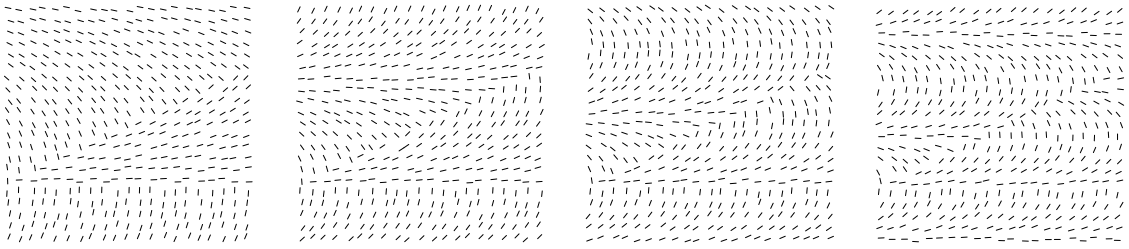

Fig. 12. With $\Delta\theta_{\text{between}}$ set to 90°, the condition $\Delta\kappa_{\text{T}} = \Delta\kappa_{\text{N}}$ consistency produces a parallel/perpendicular configuration at the orientation edge. Shown here (left to right) are the left-triangle stimuli for $\Delta\theta_{\text{within}} \in \{5°, 10°, 15°, 20°\}$.

4. Configural effects reexamined

To simplify forthcoming wording, let the *configuration hypothesis* be the observation that performance improves when texels are oriented parallel (and "to some extent perpendicular") to the perceived texture edge (Nothdurft, 1992; Wolfson & Landy, 1995). We now formalize it into a quantitative saliency measure to examine whether it is compatible with the results of Experiment 1. To do so, we assume that the orientation of the texture edge is available as a parameter, although to do so temporarily ignores the chicken-and-egg problem we mentioned above (Section 3.5). Nevertheless, the analysis is useful in several respects: (i) it provides explicit interpretation of our curvature-based findings in terms of previous configural observations, thus facilitating the comparison between them, (ii) it allows us to evaluate the configuration hypothesis for a continuum of configurations and orientation gradients, and (iii) it provides one line of investigation that leads to design of the psychophysical control experiment (see Section 5).

4.1. Formal saliency based on parallel configuration

Let θ_t denote the orientation of texels near orientation edges and let θ_e be the orientation of the edge itself. Denote by $s_t(\theta_t, \theta_e)$ the configural saliency induced by texels near the orientation edge. Since there is no agreement in the literature about the contribution of perpendicular configurations, in the following we assume that OBTS performance improves only when the orientation of texels is *parallel* to the orientation edge, a configuration which we call "parallel". Allowing graceful degradation of this improvement with changes in θ_t, we define a normalized $s_t(\theta_t, \theta_e)$ as

$$s_t(\theta_t, \theta_e) \triangleq 1 - \frac{1}{90} \cdot D_{90}(\theta_t, \theta_e), \tag{10}$$

where $D_{90}(\alpha, \beta)$ is the angular distance between the two given orientations, i.e., a number in the range $[0, 90]$ (Fig. 13A). In the rest of this paper we assume that $\theta_e = 0°$ (in accordance with the orientation edges in our stimuli), and simplify s_t to

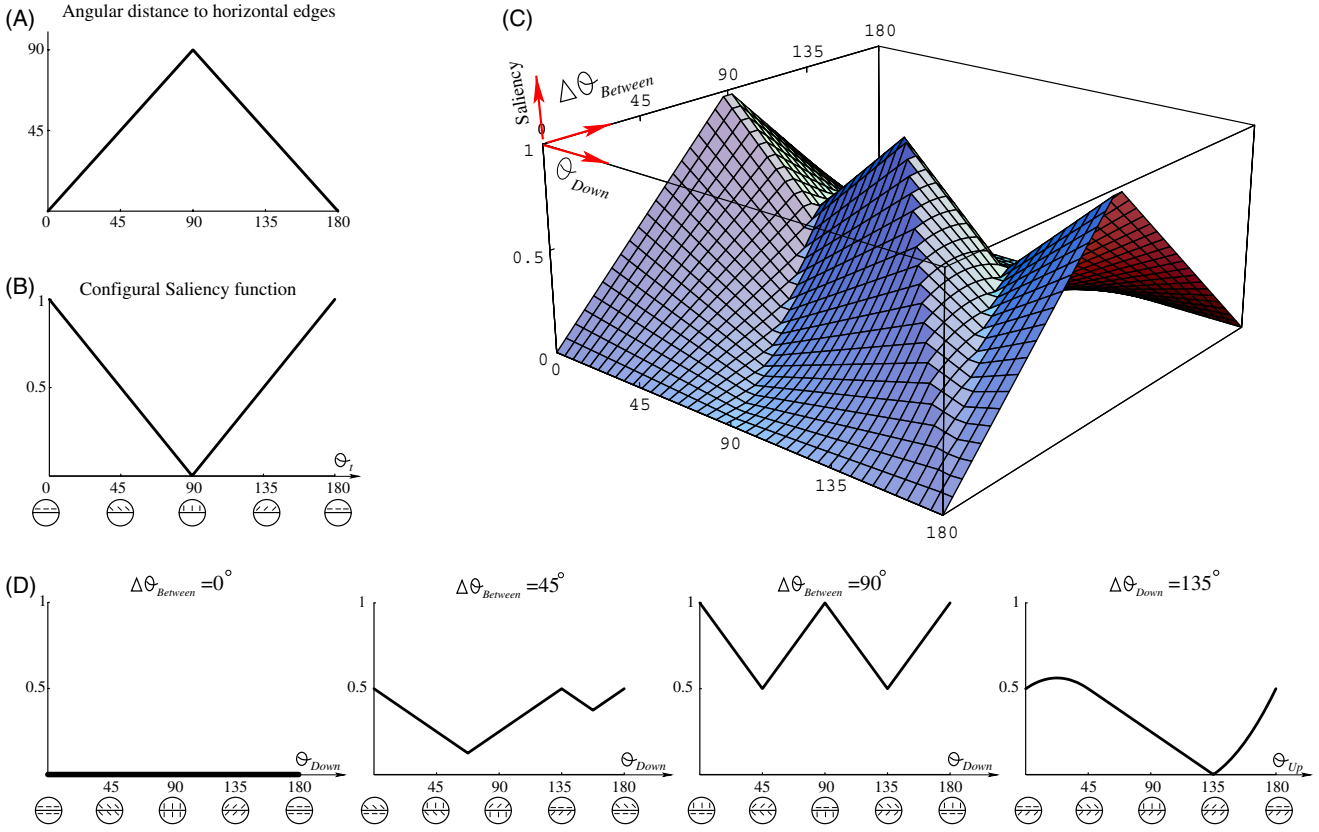

Fig. 13. Formalization of the configuration hypothesis in OBTS. (A) Since the configuration hypothesis is based on the relative angle between the orientation edge and the texture elements, some notion of "distance" between orientations is needed. We use the most natural angular distance which measures the shortest distance on the unit circle (modulo 90°). Shown here is that distance from the horizontal orientation, i.e., from 0°. (B) The saliency function (1 is most salient) based on the configuration hypothesis. Again, here we show saliency of horizontal edges. (C) The saliency function for all possible horizontal orientation edges (Eq. (12)). It vanishes for edges of $\Delta\theta_{\text{between}} = 0°$ and it peaks for parallel configurations of $\Delta\theta_{\text{between}} = 90°$. (D) Few cross sections of $S(\theta_{\text{down}}, \Delta\theta_{\text{between}})$. The three cross sections on the left correspond to fixed values of $\Delta\theta_{\text{between}}$. The cross section on the right corresponds to a fixed $\theta_{\text{down}} = 135$ and varying θ_{up} (i.e., varying $\Delta\theta_{\text{between}}$ as well). See text for comparison to psychophysical measurements in the literature (note that zero saliency level corresponds to chance level in OBTS experiments).

$$s_t(\theta_t) \triangleq 1 - \frac{1}{90} \cdot D_{90}(\theta_t, 0), \tag{11}$$

as illustrated in Fig. 13B.

By definition, any orientation edge is created by a one-dimensional discontinuity in the 2D orientation field (or function). Since our edges are horizontal, we label the orientation of the field along the two sides of the discontinuity by θ_{down} and θ_{up}. Consequently, the configural saliency of the edge is some combination of the configural saliency of the texels on the two sides of the discontinuity. An intuitive and straight forward combination is the L_∞ norm (i.e., the maximum) of the saliencies of the two sides. Incorporating also the contribution of the orientation gradient $\Delta\theta_{\text{between}}$ across the edge, we therefore model the edge's perceptual saliency $S(\theta_{\text{down}}, \theta_{\text{up}})$ in terms of θ_{down} and $\Delta\theta_{\text{between}}$ as follows (note that $\theta_{\text{up}} = \theta_{\text{down}} + \Delta\theta_{\text{between}}$):

$$S(\theta_{\text{down}}, \Delta\theta_{\text{between}}) \triangleq \frac{\Delta\theta_{\text{between}}}{90} \cdot \max\left[s_t(\theta_{\text{down}}), s_t(\theta_{\text{down}} + \Delta\theta_{\text{between}})\right]. \tag{12}$$

This function, whose parameters are (1) the texels orientation on one side of the edge, and (2) the orientation gradient across the edge, is illustrated in Fig. 13C. To examine if it is a good predictor we computed different cross-sections that correspond to previous findings in the literature (Fig. 13D). In particular, compare the cross section for $\Delta\theta_{\text{between}} = 90°$ with Fig. 12C in Wolfson and Landy (1995), or the one for $\theta_{\text{down}} = 135°$ to their Fig. 12D (or Fig. 12H, I after appropriate rotation of the X-axis).

Equipped with a quantitative model that formalizes the configuration hypothesis, we now apply it to the curvature-based stimuli used in Experiment 1, make saliency predictions with regard to them, and compare these predictions to the psychophysical results. As we show, this comparison reveals important deficiencies in the configuration hypothesis.

To apply the saliency model to the three cases of curvature discontinuities, we first find the behavior of the orientation field around the discontinuities that they induce. In other words, for each curvature discontinuity and $\Delta\theta_{\text{between}}$, we find its corresponding θ_{down} by evaluating the orientation functions in Eq. (6) at the discontinuity position, with θ_0 solved through Eq. (7) for the three cases of curvature discontinuity (Eq. (9)). This computation yields the following values, which turn out to be independent of $\Delta\theta_{\text{within}}$:

$$\begin{aligned}
\theta_{\text{down}}(\Delta\kappa_T = 0) &= -\frac{\Delta\theta_{\text{between}}}{2} - 90°, \\
\theta_{\text{down}}(\Delta\kappa_T = \Delta\kappa_N) &= -\frac{\Delta\theta_{\text{between}}}{2} - 45°, \\
\theta_{\text{down}}(\Delta\kappa_N = 0) &= -\frac{\Delta\theta_{\text{between}}}{2}.
\end{aligned} \tag{13}$$

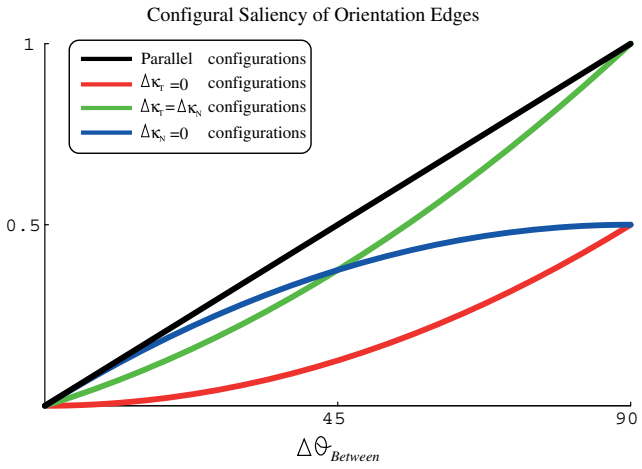

Fig. 14. The configuration-modulated saliency of orientation edges as a function of their orientation gradient $\Delta\theta_{\text{between}}$. The black graph depicts the predicted saliency of parallel configurations. The red, green, and blue graphs depict the predicted saliency of the orientation edges induces by the $\Delta\kappa_T = 0$, $\Delta\kappa_T = \Delta\kappa_N$, and $\Delta\kappa_N = 0$ edges, respectively (the three cases are color-coded similar to previous figures).

Plugged into the saliency function $S(\theta_{\text{down}}, \Delta\theta_{\text{between}})$, this evaluates the configural saliency of the edges in our stimuli, *as predicted from the configuration hypothesis*. In the same spirit, we also evaluate the predicted saliency of parallel configurations. The four resultant saliency graphs are plotted to scale in Fig. 14.

Fig. 14 is the main result of this section as it summarizes the relationship between curvature-based edges and their expected configural saliency based on the configuration hypothesis. A few observations are immediate, and most clearly is the one that, for any given $\Delta\theta_{\text{between}}$, parallel configurations (black graph) are always more salient than any of the curvature-defined edges. This confirms that the saliency measure captures what the configuration hypothesis was designed to express.

Based on Fig. 14, one can make certain predictions with regard to the *relative saliency* of the three curvature-based orientation edges used in Experiment 1. In particular, we observe the following:

P1: $\Delta\kappa_T = 0$ discontinuities are the least salient for all $\Delta\theta_{\text{between}} < 90°$,
P2: $\Delta\kappa_T = 0$ and $\Delta\kappa_N = 0$ discontinuities are equally salient for $\Delta\theta_{\text{between}} = 90°$,
P3: $\Delta\kappa_T = \Delta\kappa_N$ discontinuities are the most salient for all $\Delta\theta_{\text{between}} > 45°$,
P4: $\Delta\kappa_N = 0$ discontinuities are the most salient for all $\Delta\theta_{\text{between}} < 45°$,
P5: $\Delta\kappa_N = 0$ and $\Delta\kappa_T = \Delta\kappa_N$ discontinuities are equally salient for $\Delta\theta_{\text{between}} = 45°$.

As can be observed in Fig. 10, predictions P1 and P3 are largely confirmed by Experiment 1. The rest, however, are either wrong or depend critically on $\Delta\theta_{\text{within}}$,

in clear contradiction to the lack of such dependency in the configuration hypothesis and its derived saliency measure. In particular

- P2 appears to be correct for $\Delta\theta_{\text{within}} \geqslant 15°$ only, but not for smaller ones. For example, the relative performance at $\Delta\theta_{\text{within}} = 10°$ and $\Delta\theta_{\text{between}} = 90°$ shows clearly that the $\Delta\kappa_{\text{N}} = 0$ (blue) discontinuity is significantly more salient than the $\Delta\kappa_{\text{T}} = 0$ one.
- P4 appears to be partially correct for smaller $\Delta\theta_{\text{within}}$ but not for larger ones. For example, it is clearly wrong for $\Delta\theta_{\text{within}} = 20°$.
- P5 is wrong for $\Delta\theta_{\text{within}} > 10°$.

The observations above strongly suggest that there is a significant gap between the configuration hypothesis and performance in OBTS. It may be argued that all it takes to fix the wrong predictions, and the configuration hypothesis itself, is the incorporation of $\Delta\theta_{\text{within}}$ into Eq. (12) in a way implied by signal detection theories and recent related findings in the OBTS literature (Mussap & Levi, 1999; Nothdurft, 1991). However, doing so will reduce the saliency of *all* orientation edges by a factor proportional to $\Delta\theta_{\text{within}}$ and thus will do no more than to equally shift down (and rectify at zero) all the graphs in Fig. 14. Since such a transformation does not change the *relative* order of the graphs, the *relative* saliencies and the wrong predictions that follow from them will still hold. We conclude that even an expansion of the model to address basic signal detection concerns is insufficient to explain the results of Experiment 1.

4.2. Formal saliency based on other configuration hypotheses

The discussion in Section 4.1 revolves around the hypothesis that performance in OBTS improves when the texels' orientation is parallel to the perceived texture edge (Nothdurft, 1992; Wolfson & Landy, 1995). However, it is possible that the configural content of this hypothesis is incomplete. In fact, Wolfson and Landy themselves relaxed the conclusion, saying that "performance (in OBTS) improves when the texels' orientation is parallel, *and to some extent perpendicular*, to the perceived texture edge" (Wolfson & Landy, 1995, p. 2876, emphasis added). To examine this and other variations, we repeated the analysis of Section 4.1 for a variety of other saliency models, including models that assign some saliency weight to perpendicular configurations, and models that modulate saliency non-linearly as the configuration shifts from the optimal ones. All these models either failed to predict the previous findings of Wolfson and Landy (1995) even at the most basic levels (e.g., they failed to reproduce the correct cross sections similar to those in Fig. 13D), or they resulted in saliency predictions similar to those produced from the original model of Section 4.1. Examples of the predictions from a model that assigns some saliency to perpendicular configurations are illustrated in Fig. 15.

4.3. Discussion

The formalization of the configuration hypothesis into a saliency measure provides a basis to relate it to the curvature-based findings of Experiment 1 and leads to the conclusion that there exists a gap between the simple configural effect that this hypothesis articulates and actual performance in OBTS. Naturally, this raises the possibility that the configuration hypothesis is not explanatory even for those configurations it designates as optimal. Thus, we now wish to scrutinize the relationship, and differences in saliency, between parallel configurations and the curvature-based edges of $\Delta\kappa_{\text{T}} = \Delta\kappa_{\text{N}}$ that emerged as optimal in the conditions tested by Experiment 1. Although some data relevant to these questions may be hidden implicitly in the interaction between the saliency graphs (Fig. 14) and the curvature-based findings (Fig. 10), we next address these issues directly in Experiment 2.

To compare psychophysically two classes of stimuli whose differences are likely to be subtle, one first needs to identify those cases that maximize the differences between them. Fig. 14 suggests that the saliency of $\Delta\kappa_{\text{T}} = \Delta\kappa_{\text{N}}$ discontinuities (green graph) is somewhat less than that of parallel configurations (black graph). It shows that the differences collapse at very small and very large $\Delta\theta_{\text{between}}$, and that they are maximized at $\Delta\theta_{\text{between}} = 45°$. Fig. 14 thus implies that the best candidates for revealing differences between the two classes of stimuli are those with $\Delta\theta_{\text{between}} = 45°$. This conclusion, however, is based on the saliency measure we developed thus far, while in Experiment 2 we seek a far less constrained argument, i.e., one that is completely independent of any particular modeling step. As it turns out, even without any modeling of saliency, stimuli of $\Delta\theta_{\text{between}} = 45°$ are indeed the best candidates to probe OBTS for differences between the configuration hypothesis and curvature-based edges.

5. Experiment 2—The configuration hypothesis vs. curvature-based edges

The goal of Experiment 2 is to examine the differences in saliency between parallel configurations and orientation edges with $\Delta\kappa_{\text{T}} = \Delta\kappa_{\text{N}}$, while all other factors ($\Delta\theta_{\text{within}}$ and $\Delta\theta_{\text{between}}$) are held constant. We first observe that it makes no sense to look for possible differences for *all* values of $\Delta\theta_{\text{between}}$. As Fig. 12 and Eq. (13) show, the two cases collapse when $\Delta\theta_{\text{between}} = 90°$ (i.e., edges of maximal orientation gradient and strict parallel/perpendicular configuration also have $\Delta\kappa_{\text{T}} = \Delta\kappa_{\text{N}}$)

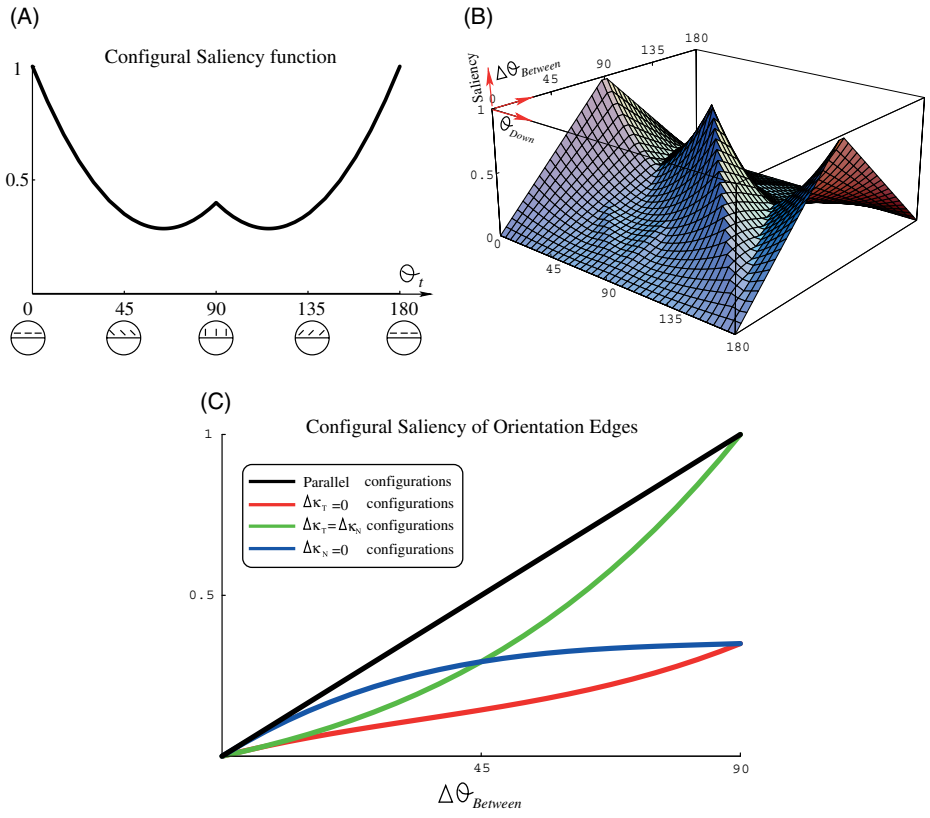

Fig. 15. The configuration-modulated saliency of orientation edges based on a saliency model that assigns some saliency to perpendicular configurations as well. (A) The saliency function of the variant model (compare to Fig. 13B). (B) The corresponding saliency function for all possible horizontal orientation edges (compare to Fig. 13C). (C) The configuration-modulated saliency of orientation edges as a function of their orientation gradient $\Delta\theta_{\text{between}}$. Different cases are color-coded similar to Fig. 14. Note that despite some perturbation in the graphs themselves, their mutual relationship and relative ordering is preserved. Thus, this saliency model, which "improves performance when texels are parallel, and to some extent perpendicular, to the perceived texture edge" (Wolfson & Landy, 1995), produces qualitatively similar predictions to those discussed in Section 4.1.

and thus no differences should be expected then. Eq. (13) shows, however, that in general, these two classes of edges will be different. To maximize the chance of detecting perceptual differences, we need to find the $\Delta\theta_{\text{between}}$ for which the differences between the two classes are also maximized. In other words, we need to find $\Delta\theta_{\text{between}}$ for which parallel configurations have curvature discontinuities which *differ the most* from the $\Delta\kappa_{\text{T}} = \Delta\kappa_{\text{N}}$ condition. For this reason we need to evaluate the curvature discontinuities induced by parallel configurations of all possible $\Delta\theta_{\text{between}}$.

Given $\Delta\theta_{\text{between}}$, we first solve Eq. (6) for θ_0 that gives rise to a parallel configuration at an arbitrary edge position $y = D$ (recall that all our orientation edges are horizontal). Since parallel configurations can be characterized by parallel texels on either side, a proper analysis should consider both the case where $\theta_{\text{ground}}(x, D) = k \cdot 180°$ and the one where $\theta_{\text{figure}}(x, D) = k \cdot 180°$, for $k \in \{0, 1, 2, \ldots\}$. As it turns out, the two cases yield the same conclusion, which is also independent of k. Thus, in the following we describe the results for parallel configurations of $\theta_{\text{ground}}(x, D) = 0°$, which implies that $\theta_0 = -D\Delta\theta_{\text{within}}$ (see Eq. (6)).

With θ_0 determined, so are θ_{ground} and θ_{figure} (Eq. (6)). Now we compute their corresponding curvature functions $\kappa_{\text{T}}(x, y)$ and $\kappa_{\text{N}}(x, y)$ from Eq. (3), subtract, and evaluate at the edge position to yield both $\Delta\kappa_{\text{T}}$ and $\Delta\kappa_{\text{N}}$:

$$\theta_{\text{ground}}(x, D) = 0 \Rightarrow \begin{cases} \Delta\kappa_{\text{T}}(x, D) = \Delta\theta_{\text{within}} \cdot \sin(\Delta\theta_{\text{between}}) \\ \Delta\kappa_{\text{N}}(x, D) = \Delta\theta_{\text{within}} \cdot [\cos(\Delta\theta_{\text{between}}) - 1]. \end{cases} \quad (14)$$

These functions are plotted against $\Delta\theta_{\text{within}}$ and $\Delta\theta_{\text{between}}$ in Fig. 16A, B.

Recall that we are looking for the conditions under which parallel configurations differ the most from the $\Delta\kappa_{\text{T}} = \Delta\kappa_{\text{N}}$ condition. This can be solved analytically by maximizing the magnitude of the difference between $\Delta\kappa_{\text{T}}(x, D)$ and $\Delta\kappa_{\text{N}}(x, D)$ in Eq. (14). The solution turns out to be $\Delta\theta_{\text{between}} = 45°$, regardless of $\Delta\theta_{\text{within}}$. The same solution is illustrated graphically in Fig. 16C and D.

We conclude that if the parallel and curvature-based configurations exhibit differences in saliency, they will be most prominent in orientation edges of $\Delta\theta_{\text{between}} = 45°$. Fig. 16 also shows that these differences are rather subtle and that they grow linearly with $\Delta\theta_{\text{within}}$.

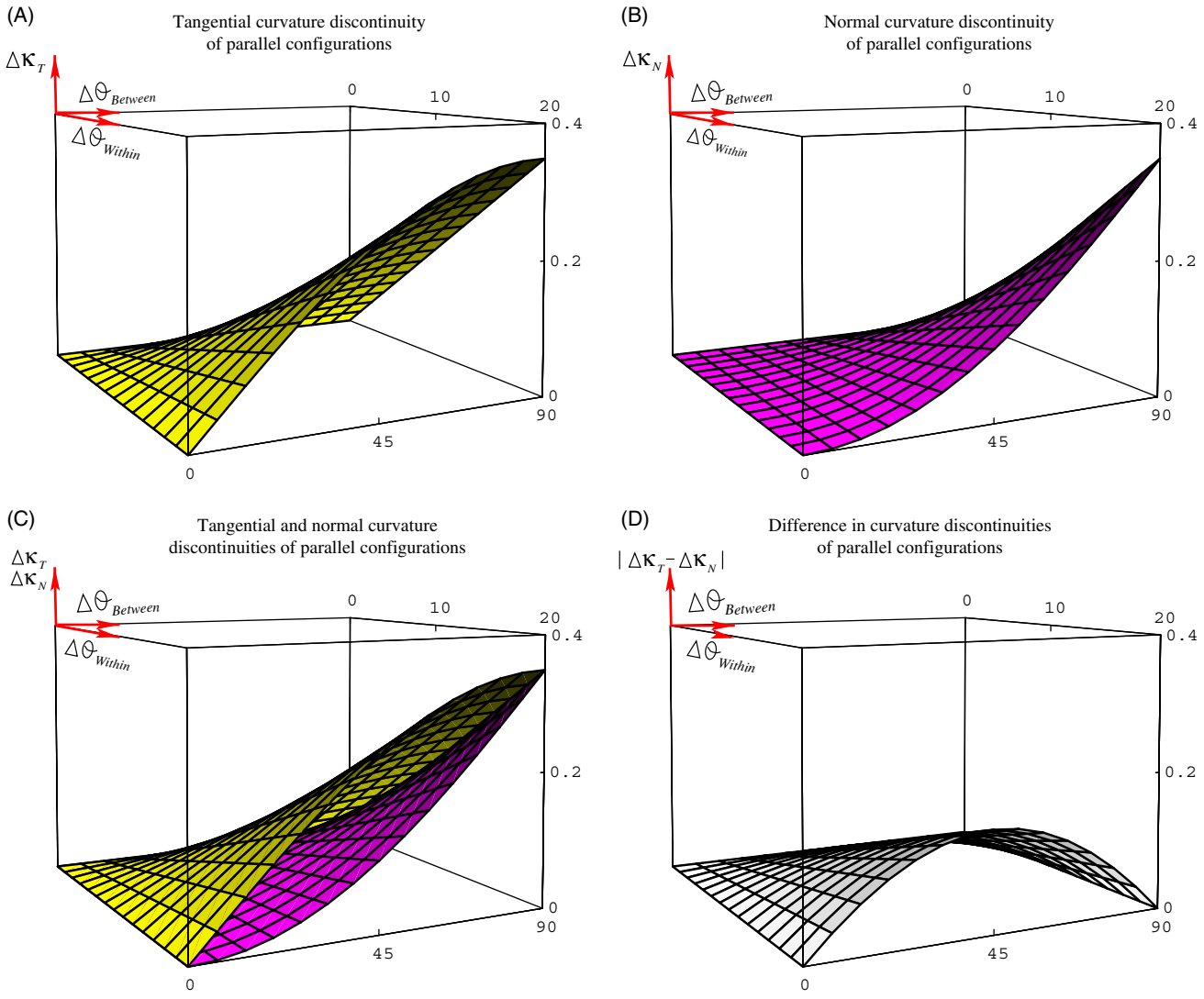

Fig. 16. Curvature discontinuities of parallel configurations as a function of $\Delta\theta_{\text{within}}$ and $\Delta\theta_{\text{between}}$. (A) Tangential curvature discontinuity $\Delta\kappa_{\text{T}}$. (B) Normal curvature discontinuity $\Delta\kappa_{\text{T}}$. (C) Superimposing both tangential and normal curvature discontinuities on the same graph shows how the difference is minimized for small and large $\Delta\theta_{\text{between}}$, while being maximized for $\Delta\theta_{\text{between}} = 45°$. (D) A graph of $|\Delta\kappa_{\text{T}} - \Delta\kappa_{\text{N}}|$ shows clearly that the difference between the two curvature discontinuities is maximized for $\Delta\theta_{\text{between}} = 45°$ (for any given $\Delta\theta_{\text{within}}$) and that it grows linearly with $\Delta\theta_{\text{within}}$.

5.1. Stimuli

Stimuli used in Experiment 2 were constructed similarly to Experiment 1, although $\Delta\theta_{\text{between}}$ was fixed at 45° (as a result of the discussion above) and $\Delta\theta_{\text{within}}$ was limited to no more than 20° (beyond which performance dropped to chance level in Experiment 1). For each $\Delta\theta_{\text{within}} \in \{5°, 10°, 15°, 20°\}$ we computed three pairs of stimuli (left- and right-pointing triangles in each pair), to cover three basic configurations: (1) parallel configuration at the figure side of the edge, (2) parallel configuration at the ground side of the edge, and (3) a curvature-based edge of $\Delta\kappa_{\text{T}} = \Delta\kappa_{\text{N}}$. Fig. 17 illustrates the six stimuli that correspond to $\Delta\theta_{\text{within}} = 5°$.

5.2. Subjects and procedure

Five subjects from those who participated in Experiment 1, took part in this experiment, and all (but one author) were naive to its purpose. All subjects had normal or corrected-to-normal vision and each ran one session of 360 trials, arranged in 10 blocks of 36 trials separated by short breaks. Each session lasted for less than 20 min and was preceded by one or two practice blocks of 72 trials. All other parameters in Experiment 2 were similar to those of Experiment 1 although now each stimulus was presented 30 times, 15 for each of the two possible figures. The presentation order was randomized and set before the experiment.

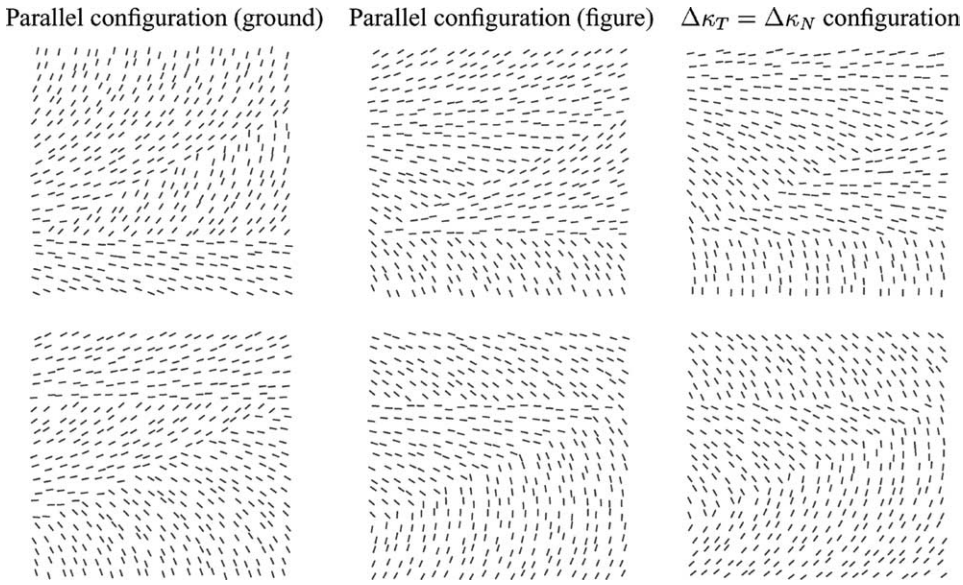

Fig. 17. Example of the stimuli used in Experiment 2, shown here for $\Delta\theta_{\text{within}} = 5°$. Similar sets were constructed for $\Delta\theta_{\text{within}} \in \{10°, 15°, 20°\}$. In all cases $\Delta\theta_{\text{between}}$ was set to 45°.

5.3. Results

To check for differences in performance between the detection of parallel configurations and those with $\Delta\kappa_T = \Delta\kappa_N$ we averaged the accuracy of detecting the two parallel configurations (cases 1 and 2 above) and subtracted from it the accuracy of detecting the $\Delta\kappa_T = \Delta\kappa_N$ configuration (case 3 above). Fig. 18 presents the average difference in performance as a function of $\Delta\theta_{\text{within}}$. It shows clearly that while parallel configurations are more salient for small $\Delta\theta_{\text{within}}$, they are less salient for larger $\Delta\theta_{\text{within}}$, where they are outperformed by the $\Delta\kappa_T = \Delta\kappa_N$ configuration.

This change in relative saliency is subtle and occurs gradually, but it was always statistically significant as soon as $\Delta\theta_{\text{within}}$ increased by more than 5° ($p < 0.01$ for $\Delta\theta_{\text{within}}$ increase of 10° and $p < 0.005$ for $\Delta\theta_{\text{within}}$ increase of 15°). The difference in the means for $\Delta\theta_{\text{within}} = 10°$ and $\Delta\theta_{\text{within}} = 15°$ was already statistically significant ($p < 0.05$) even though the increase in $\Delta\theta_{\text{within}}$ was only 5°.

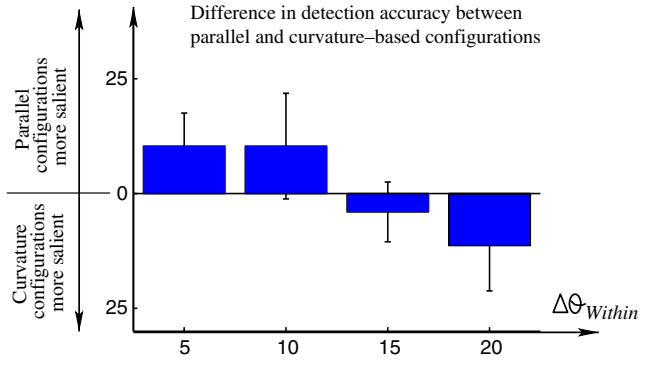

Fig. 18. Average difference in detection accuracy between parallel configurations and $\Delta\kappa_T = \Delta\kappa_N$ ones, plotted against $\Delta\theta_{\text{within}}$.

5.4. Discussion

The results of Experiment 2 clearly show that the configuration hypothesis is not generally true even for those parallel configurations which it strictly designates as optimal. It further shows clear dependency on $\Delta\theta_{\text{within}}$, in full agreement with Experiment 1 and the conclusions made Section 4. These results reinforce Experiment 1 to suggest that OBTS is indeed sensitive to curvature discontinuities when these discontinuities become significant enough (as is possible in ODTs of large $\Delta\theta_{\text{within}}$). At this point, any advantage due to the parallel configuration is overwhelmed by the effect of the curvature discontinuities. Note that these findings are also consistent with Fig. 16 which predicts that curvature discontinuities are likely to influence OBTS the most when $\Delta\theta_{\text{within}}$ is large.

6. General discussion

It was shown in the past that OBTS is influenced by the two orientation gradients $\Delta\theta_{\text{within}}$ and $\Delta\theta_{\text{between}}$ (Mussap & Levi, 1999; Nothdurft, 1991). It was further argued that OBTS is independently modulated by particular configural organizations in the neighborhood of the texture boundary (Nothdurft, 1992; Wolfson & Landy, 1995). In this paper we have shown that, in addition to the above processes, OBTS is also sensitive to discontinuities (or contrast) in two texture curvatures

$\Delta\kappa_T$ and $\Delta\kappa_N$, and it appears to improve the most when both discontinuities are maximized simultaneously, i.e., when $\Delta\kappa_T = \Delta\kappa_N$. In Section 2 we showed how the notion of curvature emerges naturally from a geometrical model of ODTs and how it is fundamentally linked to the interaction between positions and orientations. From a mathematical perspective, then, it would have been extremely surprising had an effect of curvature not been found.

It should be mentioned that the notion of "curvature discontinuities" should be understood more generally as "curvature contrasts", high "curvature gradients", or simply "rapid changes in curvatures". The perceptual equivalence of continuous (but large) gradients to pure discontinuities has been demonstrated already for orientation (e.g., Landy & Bergen, 1991) and it is more strongly applicable to higher order properties like curvature. Moreover, this equivalence is especially true for the discretized stimuli that we (and virtually all other studies in the OBTS literature) employ, since some blurring in the measurement process is necessarily implied.

The introduction of ODT curvatures into the psychophysical investigation of OBTS carries the advantage of emphasizing the spatially varying nature of ODTs and the observation that constant (or piecewise constant) ODTs are in fact accidental in natural, every-day stimuli. With curvatures, such variations in ODTs can be integrated into stimuli in a fully controlled way, thus allowing a direct link to human perception and performance.

As we discussed in the Introduction (Section 1.1), most classical studies of ODTs ignored the spatially varying nature of ODTs, focusing instead on piecewise constant structures only. Studying configural effects within this limited scope, Wolfson and Landy (1995) concluded that OBTS is improved if the orientation of texels is parallel (and to some extent perpendicular) to the texture edge. Indeed, piecewise constant ODTs have $\kappa_T = \kappa_N = 0$, their boundaries emerge solely from orientation discontinuities, and thus saliency considerations involving only boundary configuration can be attractive. As we demonstrated, such arguments also are closely related to the fold and cut organization induced by the interactions of surfaces during the imaging process.

However, in the natural world, most ODTs are spatially varying, which suggests that configural factors should be examined within a larger scope, as we further did in the current study. Indeed, we conclude that there are significant gaps between the classical configuration hypothesis (Nothdurft, 1992; Wolfson & Landy, 1995) and actual performance in OBTS. We have shown that configural effects are neither independent of spatial variations (captured, e.g., by $\Delta\theta_{within}$), nor are they universal: while parallel configurations appear superior in ODTs of small internal variation of $\Delta\theta_{within} \leqslant 10°$, larger $\Delta\theta_{within}$ results in significant texture curvatures, at which point the advantage due to parallel configurations is superseded by the one due to the curvature discontinuities. Interestingly, the results by Nothdurft (1992) may already contain a flavor of this phenomenon since the peak performance he measured deviates up to 30° from the strictly parallel configuration (see his Fig. 3A–C). Unfortunately, due to a similar deviation in the orientation of the texels themselves relative to the orientation edge, it is impossible to asses whether these findings are indicative of something other than the configuration.

The advantage of the curvature-based explanation over the one based on configural modulations is fundamental. The former is based on intrinsic data only and thus can be developed into a predictive computational mode. The latter, on the other hand, is undermined by a chicken-and-egg problem; it needs the outcome of the segmentation process (namely, the perceptual edge and its orientation) in order to make predictions about its own occurrence. In this spirit it is instrumental to re-examine Fig. 5 which we discussed in Sections 1.2 and 3.5. Fig. 19 presents the same stimulus, now with its orientation and curvature functions also depicted as height functions (see Fig. 6B). Clearly, while the orientation gradient across the square's perimeter is constant, the discontinuities in curvatures are not; they are simultaneously large only along the top edge. According to the results of Experiment 1, this edge should be the most salient, a prediction that agrees well with the perceptual evidence. Notably, this prediction does not require the orientation of the texture boundary as an input; it is made using intrinsic and local information only.

Since a main conclusion in this paper is the fact that orientation gradients are insufficient to explain OBTS, it remains to examine our results, both computational and psychophysical, in a larger context. For example, given the central role of *feature gradients* in early vision (Julesz, 1986; Nothdurft, 1993), our results justify the re-examination of feature gradients in preattentive vision more generally. Furthermore, since many other perceptual features (e.g., shading, motion, color) can be represented in terms of orientation, their intrinsic geometry, and segmentation, should be investigated analogously.

Lastly, combining our results with the observation that the complement of segmentation is visual *integration* suggests that limiting the discussion on visual integration to curves only (e.g., Field, Hayes, & Hess, 1993) may miss an important functional aspect of biological vision systems. Current "association field" models, popular in psychophysics (Field et al., 1993; Hess & Field, 1999; Kapadia, Ito, Gilbert, & Westheimer, 1995; Kapadia, Westheimer, & Gilbert, 2000), physiology

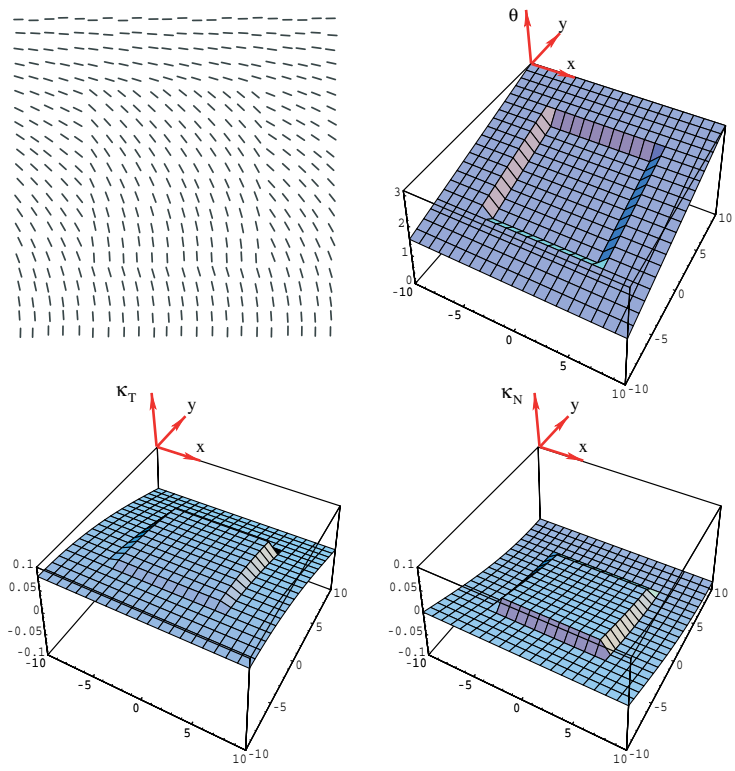

Fig. 19. Curvature discontinuities predict the saliency of orientation edges in the stimulus from this figure. Although the orientation gradient along the square's perimeter is constant (as seen best in the 3D plot), the jump in the curvatures is not. In particular, while $\Delta\kappa_T$ is virtually zero at the bottom edge, it is large, and roughly equal to $\Delta\kappa_N$, at the top edge. Thus intrinsic considerations alone can predict not only the location of edges, but their relative saliency as well.

(Bosking, Zhang, & Fitzpatrick, 1997; Kapadia et al., 1995, 2000; Schmidt, Goebel, Löwel, & Singer, 1997) and computational modeling (Parent & Zucker, 1989; Yen & Finkel, 1998), typically ignore curvature, and never consider *normal* curvature. Thus, the formal analysis and psychophysics outlined in this paper may provide the first step toward explaining the many findings which are inconsistent with curve integration, both psychophysically and physiologically (e.g., Adini, Sagi, & Tsodyks, 1997; Kisvárday, Tóth, Rausch, & Eysel, 1997; Matsubara, Cynader, Swindale, & Stryker, 1985; Polat & Sagi, 1993; Sincich & Blasdel, 2001; Ts'o, Gilbert, & Wiesel, 1986). They further provide the baseline from which other phenomena such as "edge hallucination" (Nothdurft, 1992) can be studied.

Acknowledgements

We wish to thank Paul Bourke from the Swinburne University of Technology, Australia, for the Klein bottle image in Fig. 1d. We are also thankful to the anonymous reviewer for suggesting an examination of a possible effect due to "kink" structures in the stimuli. This research was supported by AFOSR, ONR, and DARPA.

Appendix A. Glossary

θ	orientation function of the ODT
θ_{ground}	orientation function of the ODT's ground region
θ_{figure}	orientation function of the ODT's figure region
θ_{down}	ODT's orientation at the bottom side of the perceptual edge
$\Delta\theta_{\text{between}}$	scalar orientation gradient (or contrast) across a perceptual orientation edge
$\Delta\theta_{\text{within}}$	scalar orientation gradient (or contrast) within a perceptually coherent ODT region
$\nabla\theta$	vectorial orientation gradient (or contrast) within a perceptually coherent ODT region
$\|\nabla\theta\|$	magnitude of $\nabla\theta$ and an alternative way to refer to $\Delta\theta_{\text{within}}$
$\vec{\mathbf{q}}$	spatial (or retinotopic) position
$\widehat{\mathbf{E}}_T$	tangential basis vector of the ODT at any given spatial position
$\widehat{\mathbf{E}}_N$	normal basis vector of the ODT at any given spatial position
$\vec{\mathbf{V}}$	direction vector in the stimulus plane
$\nabla_{\vec{\mathbf{V}}}E$	covariant derivative of vector field E in the direction V
κ_T	tangential curvature function of an ODT
κ_N	normal curvature function of an ODT

$\Delta\kappa_T$ discontinuity in tangential curvature across a perceptual orientation edge

$\Delta\kappa_N$ discontinuity in normal curvature across a perceptual orientation edge

$\Delta\kappa_{max}$ the maximal possible discontinuity in either curvatures

D vertical spatial position of the orientation edge in our stimuli

θ_e orientation of the perceptual edge

θ_t orientation of ODT texels near the perceptual edge

$S(\cdot,\cdot)$ model function for the configural saliency of orientation edges based on the configuration hypothesis.

References

Adini, Y., Sagi, D., & Tsodyks, M. (1997). Excitatory–inhibitory network in the visual cortex: psychophysical evidence. In *Proceedings of the National Academy of Sciences of the USA* (pp. 10426–10431). Vol. 94.

Ben-Shahar, O., & Zucker, S. (2003). The perceptual organization of texture flows: a contextual inference approach. *IEEE Transactions on Pattern Analysis and Machine Intelligence, 25*(4), 401–417.

Bosking, W., Zhang, Y. B. S., & Fitzpatrick, D. (1997). Orientation selectivity and the arrangement of horizontal connections in the tree shrew striate cortex. *The Journal of Neuroscience, 17*(6), 2112–2127.

Caputo, G. (1997). Object grouping contingent upon background. *Vision Research, 37*(10), 1313–1324.

Caputo, G., & Casco, C. (1999). A visual evoked potential correlate of global figure-ground segmentation. *Vision Research, 39*, 1597–1610.

Corbit, J., & Garbary, D. (1995). Fractal dimension as a quantitative measure of complexity in plant development. In *Proceedings of the Royal Society of London, Series B* (pp. 1–6). Vol. 262.

do Carmo, M. (1976). *Differential geometry of curves and surfaces*. Prentice-Hall Inc.

Field, D., Hayes, A., & Hess, R. (1993). Contour integration in the human visual system: evidence for a local 'association' field. *Vision Research, 33*, 173–193.

Hess, R., & Field, D. (1999). Integration of contours: new insights. *Trends in Cognitive Sciences, 3*, 480–486.

Hubel, D., & Wiesel, T. (1977). Functional architecture of macaque monkey visual cortex. In *Proceedings of the Royal Society of London, Series B* (pp. 1–59). Vol. 198.

Huggins, P., & Zucker, S. (2001). Folds and cuts: how shading flows into edges. In *Proceedings of the IEEE international conference on computer vision*.

Julesz, B. (1981). Textons, the elements of texture perception, and their interactions. *Nature, 290*(12), 91–97.

Julesz, B. (1986). Texton gradients: the texton theory revisited. *Biological Cybernetics, 54*, 245–251.

Kanizsa, G. (1979). *Organization in vision: essays on Gestalt perception*. Praeger Publishers.

Kapadia, M., Ito, M., Gilbert, C., & Westheimer, G. (1995). Improvement in visual sensitivity by changes in local context: parallel studies in human observers and in V1 of alert monkeys. *Neuron, 15*, 843–856.

Kapadia, M., Westheimer, G., & Gilbert, C. (2000). Spatial distribution of contextual interactions in primary visual cortex and in visual perception. *Journal of Neurophysiology, 84*, 2048–2062.

Kisvárday, Z., Tóth, É., Rausch, M., & Eysel, U. (1997). Orientation-specific relationship between populations of excitatory and inhibitory lateral connections in the visual cortex of the cat. *Cerebral Cortex, 7*, 605–618.

Koenderink, J. (1990). *Solid shape*. Cambridge, MA: MIT Press.

Kruth, W. (Ed.). (1963). *The complete woodcuts of Albrecht Dürer*. Dover Publications.

Kwan, L., & Regan, D. (1998). Orientation-tuned spatial filters for texture-defined form. *Vision Research, 38*, 3849–3855.

Landy, M., & Bergen, J. (1991). Texture segregation and orientation gradient. *Vision Research, 31*(4), 679–691.

Li, Z. (1998). A neural model of contour integration in the primary visual cortex. *Neural Computation, 10*, 903–940.

Malik, J., & Perona, P. (1990). Preattentive texture discrimination with early vision mechanisms. *Journal of the Optical Society of America, 7*(5), 923–932.

Marr, D. (1982). *Vision*. WH Freeman and Company.

Matsubara, J., Cynader, M., Swindale, N., & Stryker, M. (1985). Intrinsic projections within visual cortex: evidence for orientation specific local connections. In *Proceedings of the National Academy of Sciences of the USA* (pp. 935–939). Vol. 82.

Motoyoshi, I., & Nishida, S. (2001). Visual response saturation to orientation contrast in the perception of texture boundary. *Journal of the Optical Society of America, 18*(9), 2209–2219.

Murray, J. (1989). *Mathematical biology*. Springer-Verlag.

Mussap, A., & Levi, D. (1999). Orientation-based texture segmentation in strabismic amblyopia. *Vision Research, 39*, 411–418.

Nothdurft, H. (1985a). Orientation sensitivity and texture segmentation in patterns with different line orientation. *Vision Research, 25*(4), 551–560.

Nothdurft, H. (1985b). Sensitivity for structure gradient in texture discrimination tasks. *Vision Research, 25*(12), 1957–1968.

Nothdurft, H. (1991). Texture segmentation and pop-out from orientation contrast. *Vision Research, 31*(6), 1073–1078.

Nothdurft, H. (1992). Feature analysis and the role of similarity in preattentive vision. *Perception & Psychophysics, 52*(4), 255–275.

Nothdurft, H. (1993). The role of features in preattentive vision: comparison of orientation, motion, and color cues. *Vision Research, 33*(14), 1937–1958.

Olson, R., & Attneave, F. (1970). What variables produce similarity grouping? *American Journal of Psychology, 83*, 1–21.

O'Neill, B. (1966). *Elementary differential geometry*. Academic Press.

Parent, P., & Zucker, S. (1989). Trace inference, curvature consistency, and curve detection. *IEEE Transactions on Pattern Analysis and Machine Intelligence, 11*(8), 823–839.

Polat, U., & Sagi, D. (1993). Lateral interactions between spatial channels: suppression and facilitation revealed by lateral masking experiments. *Vision Research, 33*(7), 993–999.

Regan, D., Hajdur, L., & Hong, X. (1996). Two-dimensional aspect ratio discrimination for shape defined by orientation texture. *Vision Research, 36*(22), 3695–3702.

Schmidt, K., Goebel, R., Löwel, S., & Singer, W. (1997). The perceptual grouping criterion of colinearity is reflected by anisotropies in the primary visual cortex. *The European Journal of Neuroscience, 9*, 1083–1089.

Sincich, L., & Blasdel, G. (2001). Oriented axon projections in primary visual cortex of the monkey. *The Journal of Neuroscience, 21*(12), 4416–4426.

Stevens, K. (1981). The visual interpretation of surface contours. *Artificial Intelligence, 17*, 47–73.

Todd, J., & Reichel, F. (1990). Visual perception of smoothly curved surfaces from double-projected contour patterns. *Journal of Experimental Psychology: Human Perception and Performance, 16*(3), 665–674.

Ts'o, D., Gilbert, C., & Wiesel, T. (1986). Relationships between horizontal interactions and functional architecture in cat striate

cortex as revealed by cross-correlation analysis. *The Journal of Neuroscience, 6*(4), 1160–1170.

Turing, A. (1952). The chemical basis of morphogenesis. *Philosophical Transactions of the Royal Society B (London), 237*, 37–72.

Wolfson, S., & Landy, M. (1995). Discrimination of orientation-defined texture edges. *Vision Research, 35*(20), 2863–2877.

Wolfson, S., & Landy, M. (1998). Examining edge- and region-based texture analysis mechanisms. *Vision Research, 38*(3), 439–446.

Yen, S., & Finkel, L. (1998). Extraction of perceptually salient contours by striate cortical networks. *Vision Research, 38*(5), 719–741.